AIAA JOURNAL
Vol. 46, No. 2, February 2008

Current Status of Jet Noise Predictions Using Large-Eddy Simulation

Daniel J. Bodony* and Sanjiva K. Lele†
Stanford University, Stanford, California 94305-3035

DOI: 10.2514/1.24475

A survey of the current applications of large-eddy simulation for the prediction of noise from single stream turbulent jets is given. After summarizing the numerical techniques used, the data predicted by the simulations are given at conditions from subsonic, heated jets to supersonic, unheated jets. Mach numbers between 0.3 and 2.0 are considered. Following the data presentation, an analysis of the trends exhibited by the data is given, with special attention paid to relationship between numerical and/or modeling choices and the prediction accuracy. The data support the conclusion that the most limiting factor in current large-eddy simulations is the thickness of the initial shear layer, which is commonly one order of magnitude thicker than what is found experimentally. There is also a large amount of uncertainty regarding the influence of the subgrid scale model on the predictions. The influence of inflow conditions is discussed in depth. Uncertainties in the inflow conditions currently prohibit the simulations from reliably predicting the potential core length. The centerline evolution of the mean and fluctuating axial velocity is strongly coupled to the resolution of the initial shear layers, but can be made to agree within experimental uncertainty when sufficiently thin initial shear layers are used. The maximum achieved Strouhal number of the sound in the acoustic far field is 1.5–3.0, depending on flow condition; this limit is due to numerical resources. A listing of some of the open questions and future directions concerning jet noise predictions using large-eddy simulation concludes the survey.

I. Introduction

THE desire to more reliably predict the noise reduction available to individual jet engine design concepts has led to the introduction of large-eddy simulation (LES) techniques to jet noise problems. In particular, the noise radiated by the jet engine exhaust (historically called "jet noise") has received significant attention. Though this paper deals primarily with jet noise, much of the discussion applies to other problems of engineering interest. (See also the recent paper by Wang et al. [1].) Directly predicting the radiated noise from a turbulent compressible flow and correctly capturing the acoustic propagation over distances on the order of 10 wavelengths requires the LES practitioner to carefully choose the numerical discretization in space and time. Boundary conditions in aeroacoustic simulations equally require careful selection so that, where needed, outward-traveling acoustic, entropic, and vortical waves are not reflected back into the computation domain as spurious numerical waves or as sound. Additionally, it has been found, as will be discussed next, that the inlet/inflow boundary conditions, where the initial conditions of the jet are set, have direct but poorly understood links to the near-field turbulence and the resulting acoustic radiation. The inflow conditions must also not generate spurious sound which may overwhelm the physically relevant sound. The influence of the subgrid scale model is also crucial.

The purpose of this paper is to describe, to the extent permitted by the available data, the status of the capabilities of LES with regard to the direct prediction of jet engine exhaust noise. By comparing the various available LES data to a common set of experimental data, the paper aims to highlight the correspondence between numerical choices, i.e., discretization, boundary conditions, etc., and the resulting accuracy of the predictions. There are many questions that have not yet received a completely satisfactory answer and a brief discussion of these will be given. The limited amount of available data does not permit us to definitively conclude the cause-and-effect relationship between the numerical/modeling choices and the resulting predictive accuracy. Where needed, we supplement the data by physical reasoning and scaling arguments.

It is noted that only those prediction efforts that directly capture the radiated noise are included in this paper. To compare the results obtained by various groups, only jets issuing from a single axisymmetric nozzle are considered. For low-speed jets, with Mach numbers less than 0.5, there have been studies that use the Lighthill acoustic analogy [2,3] to account for the sound generation in an incompressible calculation. These calculations are not covered in this paper but the reader is referred to [4,5] and the references therein for additional information. Likewise, those LES calculations of turbulent, compressible jets that do not include a noise prediction [6–12] are not included.

Given a selection of the available data, the paper continues by listing the numerical methods commonly used in the LES calculations, followed by a brief discussion of the boundary conditions in use. Details on the turbulent near field and acoustic far field are then given using a limited set of the quantities available. Only the mean axial velocity and its root mean square in the near field, and the acoustic overall sound pressure levels (OASPLs) and spectra in the far field, will be used. These quantities were chosen for two primary reasons: 1) they are the data most commonly reported by the simulations' authors, and 2) their experimental characterization is well established. In limiting discussion to these quantities, it is not possible to review every aspect of a set of simulations; doing otherwise would be prohibitive. Comparison of turbulence (temporal and/or spatial) spectra in the jet would be a useful way to more deeply evaluate the available simulations, but such data have not been reported by all authors.

Following presentation of the data is a brief discussion of the data and of the open questions and future directions of jet noise predictions using LES.

II. Survey of Numerical Approaches

There exists a substantial body of literature available on the large-eddy simulation of compressible, turbulent jets. The subset of these

Presented as Paper 0468 at the 44th Aerospace Sciences Meeting and Exhibit, Reno, NV, 9–12 January 2006; received 6 April 2006; revision received 11 September 2007; accepted for publication 12 September 2007.

*Center for Turbulence Research; currently Department of Aerospace Engineering, University of Illinois at Urbana–Champaign; bodony@uiuc.edu. AIAA member.

†Departments of Aeronautics and Astronautics and Mechanical Engineering; lele@stanford.edu. AIAA member.

studies that include noise predictions is considerably smaller. Early studies considered conditions of direct engineering interest [13] of high velocity, high temperature jets. More idealized jets of lower velocity, single stream, axisymmetric (in the mean) followed and attention focused on the Mach 0.9, unheated jet [9,10,14] for which a direct numerical simulation [15] and low-Reynolds-number laboratory experiment [16] also exist. Bogey et al. (BBJ) [14,17] appear to be the first to successfully predict the near field of the Mach 0.9 jet at a moderate Reynolds number using a constant coefficient Smagorinsky model (CSM), with estimates made of the far-field sound. Zhao et al. (ZFM) [18] obtained similar results using the dynamic Smagorinsky model (DSM) and a Kirchhoff surface for the far-field noise prediction.

After 2001, jet simulations at other operating conditions and detailed studies of numerical techniques and treatments, e.g., boundary conditions and subgrid scale models, appeared in the literature. Morris et al. (MLSB) [19] investigated high-speed jets with constant acoustic Mach number $M_a = U_j/a_\infty = 1.5$ at heated and unheated conditions and observed the influence of inlet conditions on the radiated sound. This latter operating condition was also independently noted by Bodony and Lele (BL) [20]. Bogey and Bailly (BB) systematically investigated, in a series of papers, the role of inflow conditions [21,22], subgrid scale modeling effects [23], and Mach and Reynolds number effects [24,25]. Andersson et al. (AED) [26,27], with the nozzle geometry included, investigated an unheated $M_a = 0.75$ jet, with a heated jet appearing later [28,29]. AED also considered inflow condition and subgrid scale model effects on the radiated sound [30]. Shur et al. (SSS) [31] considered off-design jets (pressure mismatched supersonic jets) and jets with synthetic chevrons, with additional detail and simulated conditions in [32,33]. Bodony and Lele [34,35] investigated heated and unheated subsonic and supersonic jets. Uzun et al. (UBL) [36–39] investigated the Mach 0.9 unheated jet at two moderate-to-high Reynolds numbers. Following UBL, Lew et al. (LBL) investigated inflow forcing effects [40] and subsonic heated jets [41]. Wu et al. [42] have recently considered the nozzle influence on the radiated sound.

A summary of the data used in the paper to follow, organized by acoustic Mach number M_a and static temperature ratio T_j/T_∞, is given in Table 1 (authors are listed in alphabetical order). In selecting these data, the choice was made to use those conditions that have appeared more than once in the literature so that comparisons could be made. There are other jet noise calculations, particularly by Gamet and Estivalezes [13] and Shur et al. [33], which are singular in their conditions and are thus not reported here.

Table 1 Summary of the data used

Authors	M_a	M_j	T_j/T_∞	Re_D
Mach 0.5, heated, $M_j \approx 0.4$				
Bodony and Lele (BL) [35]	0.5	0.38	1.76	27,000
Lew et al. (LBL) [41]	0.5	0.38	1.76	223,000
Shur et al. (SSS) [33]	0.5	0.27	3.40	10,000
Mach 0.5, unheated, $M_j \approx 0.5$				
Bodony and Lele [35]	0.5	0.51	0.95	79,000
Bogey and Bailly (BB) [25]	0.6	0.60	1.00	270,000
Shur et al. [33]	0.5	0.50	1.00	10,000
Mach 0.9, heated, $M_j \approx 0.5$				
Andersson et al. (AED) [30]	0.75	0.53	2.00	50,000
Bodony and Lele [35]	0.9	0.55	2.70	13,000
Lew et al. [41]	0.9	0.55	2.70	200,000
Shur et al. [43]	0.9	0.55	2.70	1,000,000
Mach 0.9, unheated, $M_j \approx 0.9$				
Andersson et al. [30]	0.75	0.75	1.00	50,000
Bodony and Lele [35]	0.83	0.90	0.86	88,000
Bogey et al. (BBJ)[17]	0.9	0.90	1.00	65,000
Shur et al. [33]	0.9	0.90	1.00	50,000
Shur et al. [33]	0.9	0.90	1.00	500,000
Uzun et al. (UBL) [39]	0.9	0.90	1.00	400,000
Zhao et al. (ZFM) [18]	0.83	0.90	0.86	3600
Mach 1.5, heated, $M_j \approx 1.0$				
Bodony and Lele [35]	1.47	0.97	2.30	84,000
Shur et al. [43]	1.63	1.00	2.67	2,000,000
Mach 1.5, unheated, $M_j \approx 2.0$				
Bodony and Lele [35]	1.47	1.95	0.56	336,000
Morris et al. (MLSB) [19]	1.47	1.95	0.56	100,000
Shur et al. [33]	1.37	1.37	1.00	500,000

A. Discretization Choices

In this section, the three categories of numerical techniques used in the simulations are presented: 1) spatial discretization, 2) temporal discretization, and 3) subgrid scale model. Each category is discussed separately.

1. *Spatial Discretization*

Both the finite volume and finite difference approaches to the approximation of spatial derivatives are employed in the studies under consideration. Early efforts, which focused on simple, "academic" geometries, used high-order finite difference schemes of both explicit and implicit (Padé) types. Particular attention was paid to the dispersion/dissipation properties of the spatial schemes. A more thorough review of such schemes is given by Colonius and Lele [44] but a brief description is given here. The essential idea is to find those coefficients $\{\alpha, \beta, \{a_i\}_{i=0}^N\}$ in

$$\beta(f'_{i-2} + f'_{i+2}) + \alpha(f'_{i-1} + f'_{i+1}) + f'_i = a_0 f_i + \sum_{j=1}^{N} a_j (f_{i+j} - f_{i-j}) \tag{1}$$

that most closely approximate the spatial derivative of f evaluated at point x_i, i.e., f'_i, in some sense. For the explicit scheme one takes $\alpha = \beta \equiv 0$. What constitutes "most closely approximates" is subjective and determines the particular scheme. For example, UBL, LBL, and ZFM use the standard sixth-order Padé approximation [45] which yields a minimally sized finite difference stencil that is sixth-order accurate and tridiagonal ($\beta \equiv 0$).[‡] BL, on the other hand, select a pentadiagonal scheme with $N = 3$. Although this scheme can potentially be tenth-order accurate, the order of accuracy is relaxed to six and the remaining two free coefficients are selected to maximize the resolution, in terms of the modified wave number, of the approximation[§] Their scheme was originally developed by Lui and Lele [46] for spatially evolving mixing layers.

BBJ have chosen the so-called dispersion-relation-preserving (DRP) family of explicit finite difference schemes originally developed by Tam and Webb [47] for approximation of the spatial derivative. Here, the coefficients $\{a_i\}_{i=0}^N$, with $\alpha = \beta \equiv 0$, are determined by considering the spatial discretization in the Fourier space and requiring a given order of accuracy, and that the numerical modified wave number closely approximates the exact wave number relation. The only differences between the Tam and Webb DRP schemes and those determined by Lui and Lele [46] are the former's restriction to explicit stencils and in how the modified wave number optimization is chosen. In their later work, Bogey and Bailly have developed DRP-like schemes with increased resolving power [48].

In contrast to finite difference methods, Andersson et al. [29] and Shur et al. [32] have employed finite volume schemes with both groups citing the need for complex geometries. Indeed, the simulations by Andersson et al. [29] and Shur et al. [32] include the nozzle geometry directly in the calculation and are unique in this aspect. In the flux reconstruction, Andersson et al. [29] use a third-order polynomial with upwinding whose coefficients have been chosen to minimize the dissipation inherent in typical upwind schemes. In a similar manner, the finite volume scheme of Shur et al. [32] uses a hybrid Roe flux-difference splitting algorithm [49] with a fourth-order central representation combined with a fifth-order

[‡]For an nth-order accurate scheme, it is implied that as Δx, the grid spacing, approaches zero, one has $|\mathrm{d}f/\mathrm{d}x(x_i) - f'_i| \sim C(\Delta x)^n$ where C is a coefficient independent of Δx.

[§]The "modified wave number" is determined by a spatial-Fourier analysis of the numerical scheme. See, for example, Lele [45].

upwind representation with the fluxes computed in a MUSCL approach [50]. The upwind biasing weight is selected visually and is a function of space: near the jet centerline the value is low for a more central scheme, whereas near the computational boundaries, a more upwinded scheme is permitted. In general, the finite volume schemes have less resolving power and are more dissipative than their counterpart high-order finite difference schemes; however, they permit complex geometries easily.

2. *Temporal Discretization*

Selection of the temporal discretization, or time integration, by the different groups falls along lines similar to the spatial discretization. For the most part, Runge–Kutta-like (RK) schemes have been used. AED use a slightly modified second-order accurate RK scheme, whereas ZFM, UBL, and LBL use the standard fourth-order RK scheme. The DRP-optimized RK algorithms of Tam and Webb have been adopted by BBJ (with additional development in [25]). BL use the low-dispersion/low-dissipation form of the RK schemes developed by Hu et al. [51]. SSS, in contrast, use an implicit second-order time advancement with inner-loop iterations to convergence.

3. *Subgrid Scale Model*

Unlike the selection of spatial and temporal discretizations, which, in one form or another, attempt to optimally represent the required derivatives, the use, or avoidance altogether, of a subgrid scale model is an open research question. The types of subgrid scale "closures" (with quotes used to generalize the notion of closure) are generally of three types: 1) constant coefficient, 2) dynamic coefficient, and 3) no model in conjunction with numerical dissipation/explicit filtering. It is item 3 that requires the generalization of the definition of closure. There is much debate about the effects a particular subgrid scale closure has on the jet turbulence and the radiated sound; a cause-and-effect discussion in this regard will be deferred until later in this article. At present, the basics of the approaches are presented to facilitate the later comparisons.

For items 1 and 2, the role of a subgrid scale closure is to approximate the subgrid scale stresses, i.e., those stresses applied to the resolved scales of motion by the unresolved scales, using only resolved scale (and possibly grid) information. A more detailed discussion of LES subgrid scale models may be found in the paper by Meneveau and Katz [52], but the basic idea is as follows. After the governing equations are filtered, there exist additional terms resulting from the nonlinear terms. Strictly speaking, the nonlinearity exists in both the convective and in the viscous terms but it is usual practice to ignore the effects of subgrid scale fluctuations in temperature on the viscous coefficients. Thus, for a typical convective term $u_i u_j$, one has the decomposition (with an overbar denoting a spatial filter operation)

$$\overline{u_i u_j} = \bar{u}_i \bar{u}_j + \tau_{ij} \tag{2}$$

where τ_{ij} is the subgrid scale stress. For the Smagorinsky [53] class of closures, one typically writes the trace-free portion of τ_{ij} as a function of the deviatoric resolved strain rate $\bar{S}^d_{ij} = \bar{S}_{ij} - \frac{1}{3}\bar{S}_{kk}\delta_{ij}$ with $\bar{S}_{ij} = (\partial \bar{u}_i/\partial x_j + \partial \bar{u}_j/\partial x_i)/2$ as

$$\tau^d_{ij} = C_s \Delta^2 \bar{S}^d_{ij} |\bar{S}| \tag{3}$$

where $|\bar{S}| = (2\bar{S}^d_{ij}\bar{S}^d_{ij})^{1/2}$ is the norm of the resolved strain rate. Here, Δ is a measure of the local grid spacing, often taken as $\Delta = (\Delta x \Delta y \Delta z)^{1/3}$ but other choices are possible, and C_s is the Smagorinsky coefficient. In a constant coefficient model, the value of C_s, along with the values of other model constants, are chosen a priori and are usually based on the model's performance on canonical flows. This is the approach taken by AED (who used the model by Erlebacher et al. [54]) and in the early work of BBJ who used the standard Smagorinsky model [53].

Alternatively, the coefficient C_s may be determined dynamically, e.g., as part of the calculation, using a dynamic procedure based on the Germano et al. identity [55]. In this approach, the value of C_s, and the other model coefficients needed in a compressible flow [56], are determined in a least-squares solution of an overdetermined linear system. Such is the technique used by BL, by MLSB (who also used a constant coefficient model), by UBL, and by ZFM. In the last aforementioned study, the dynamic mixed model (DMM) of Salvetti and Banerjee [57], where a scale-similarity contribution is combined with the dynamic Smagorinsky model, was also used.

The simulations of SSS, LBL, and the later work of BB, and UBL, do not use a subgrid scale model in the historical sense, but take the point of view that because the subgrid scale model's dominant contribution to the resolved scale dynamics is dissipative, the same result may be affected by instead using explicitly dissipative numerics. The two forms the numerical dissipation used are 1) a high-wave number filter applied to each time step to dissipate, or damp, scales of motion with wave number above some threshold (BB and LBL), and 2) numerical dissipation through upwinding (SSS).

The high wave number filters used by BB and by LBL are based on a development similar to that used in designing the finite difference schemes discussed in Sec. II.A.1. Instead of requiring an approximation to a derivative, the object of interest is a low-pass filtered version $\hat{f}$ of the original field f. The basic design consists of finding the coefficients $\{\alpha_f, \beta_f, \{b_i\}_{i=0}^N\}$ in

$$\begin{aligned}\beta_f(\hat{f}_{i-2} + \hat{f}_{i+2}) + \alpha_f(\hat{f}_{i-1} + \hat{f}_{i+1}) + \hat{f}_i \\ = b_0 f_i + \sum_{j=1}^{N} b_j (f_{i+j} + f_{i-j})\end{aligned} \tag{4}$$

that produce a numerical filter with the desired transfer function when viewed in wave number space. In the case of UBL and LBL, the tridiagonal scheme of Visbal and Gaitonde [58], with $\alpha_f = 0.47$ and $\beta_f \equiv 0$, is used. Bogey and Bailly use an optimized explicit ($\alpha_f = \beta_f \equiv 0$) filter developed in [48]. ZFM used an explicit filter for numerical stability but do not quote its effect. BL used a Padé filter for numerical stability and demonstrate independence of their predictions to the filter.

SSS, by contrast, let the dissipation of the upwinding portion of their hybrid finite volume scheme provide the necessary removal of under- and unresolved scales of motion from the calculation. This approach is similar to the MILES (monotonically integrated large-eddy simulation) method used extensively by Fureby and Grinstein [59], for example. When an explicit subgrid scale model is not used, significant computational cost savings can result. For example, UBL quote a one-third reduction in wall clock time.

B. Boundary Conditions

Focus is now placed on the boundary conditions used in the jet noise calculations under consideration. Because a primary objective of the simulations is the direct prediction of turbulence-generated noise, the boundary conditions used must not perceptively alter the radiated sound field. For lateral and outflow boundaries, this implies that acoustic reflection off the computational boundary must be minimal, i.e., nonreflecting boundaries, and at the inflow where the jet parameters are set, and disturbances possibly injected, parasitic noise must not be generated. Proper (in the sense of performance and practical application) boundary conditions remain an active research field, especially with regard to nonreflecting boundaries. The paper by Colonius [60] provides an introduction to the methods available and their relative performance. For jet noise simulations, the presentation is divided into two categories: nonreflecting boundaries and inflow boundaries (see also Fig. 1).

1. *Nonreflecting Boundaries*

The nonreflecting boundary conditions used in the majority of the jet noise simulations are roughly of a similar class, being characteristics-based for inward- and outward-traveling waves. These include the calculations of AED, BL, BBJ, LBL, UBL, and ZFM. The radiation boundary conditions of Tam and Dong [61] have been used by BBJ, LBL, and UBL. Bogey and Bailly extended the

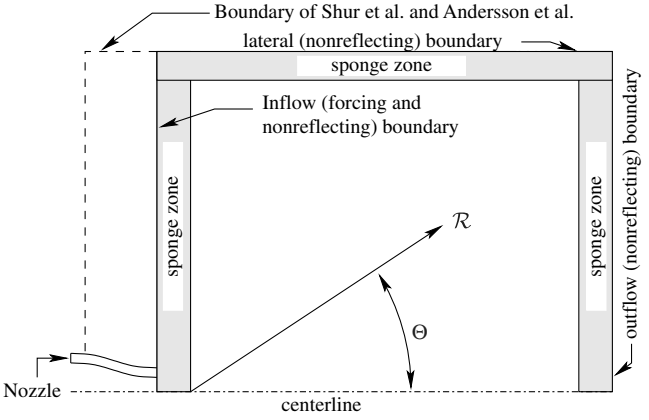

Fig. 1 Schematic of typical jet noise calculation showing inflow, lateral, and outflow boundaries. Some simulations use absorbing or sponge layers which are also shown.

Tam and Dong [61] conditions to three dimensions in [62]. ZFM used Poinsot–Lele boundary conditions [63], and AED and BL used purely characteristic boundary conditions [50].

Concurrent with the nonreflecting boundary conditions, which are only approximately nonreflecting for waves of general orientation [44], an absorbing, or sponge, zone was placed adjacent to the boundary as depicted in Fig. 1. In the absorbing layer, a "cooling" term of the form

$$-\sigma(q - q_{\text{ref}})$$

is added to the right-hand side of the governing equations. With $\sigma > 0$ only in a limited region, the additional term drives the computed solution q to a previously determined reference solution q_{ref}. When the sponge strength σ smoothly varies from $\sigma = 0$ within the domain of interest to a positive value near the boundary, the result is a relaxation of q toward q_{ref} [64]. Thus, when an acoustic wave, say, approaches a nonreflecting boundary, the wave is first attenuated by the term $-\sigma(q - q_{\text{ref}})$. A portion of wave is reflected at the computational boundary and is again attenuated as it re-traverses the sponge layer. The resulting reflected wave is usually negligible, if present at all.

The choice of σ is an open question, but a common form is

$$\sigma(\boldsymbol{x}) = A\left(\frac{x - x_1}{x_2 - x_1}\right)^n \tag{5}$$

for a sponge beginning at $x = x_1$ and ending at $x = x_2$. Typically, $n = 3$ and A is of order c_∞ / D_j.

For the reference solution q_{ref}, there is also flexibility in selection, but a common choice is to take the steady solution from a Reynolds-averaged Navier–Stokes (RANS) calculation for a jet at the same operating conditions. When the RANS solution is used, the reference solution contains a good approximation of the time-averaged entrainment required by the turbulent jet due to its lateral downstream growth. Proper accounting for the entrained fluid is necessary for realistic jet development [65].

SSS, in contrast, use extrapolation boundary conditions on the lateral edges and zero x-derivative conditions at the outflow (downstream) boundary. Though these conditions are reflecting, they are prefaced by absorbing layers as previously described with the reference solution taken as the RANS solution of the corresponding axisymmetric jet. Additional dissipation occurs as their numerical method switches to a more upwinded stencil and the grid is coarsened near the boundary, further attenuating any reflected waves.

2. *Inflow Boundaries*

At the inflow boundary, where the mean jet conditions are set, there is no apparent consensus regarding the necessity, or even appropriateness, of the explicit prescription of forcing any unsteadiness to encourage turbulence development. The division between groups lies on the inclusion (AED and SSS) or the exclusion of an explicit nozzle geometry. When the nozzle geometry is included, it is argued, the nozzle lip provides the necessary receptivity location for generated and reflected acoustic waves to scatter into vortical, entropic, and acoustic disturbances within the jet's initial shear layers. In doing so, any specification of forcing parameters is not necessary and the implicit dependence of the jet turbulence and sound field on the forcing is absent. This point of view requires, it seems, at least some reflected acoustic waves to exist within the domain during the simulation startup period to initially excite the jet. Once the initial transients have exited the domain, the upstream-traveling acoustic waves generated by the jet appear to be primarily responsible for the continued jet development of convectively unstable jets [66,67].

For those calculations without an explicit nozzle treatment, some forcing of the jet is necessary to promote natural transition from an initially quasi-laminar annular shear layer. The introduction of disturbances can potentially create parasitic noise that corrupts the physical acoustic field [10]. To avoid this, two primary methods of disturbance creation are used that apply unsteady forcing to a region in the early jet development near the computational inlet. One version uses the "vortex ring" forcing developed by BBJ wherein solenoidal disturbances of the form

$$\left\{\begin{matrix} u' \\ v' \end{matrix}\right\} = \alpha U_j \sum_{i=n}^{m} \epsilon_i \cos(i\theta + \phi_i) \times \frac{2r_0}{r\Delta y} \exp\left[-\ell_n 2 \frac{(x - x_0)^2 - (r - r_0)^2}{(\Delta y)^2}\right] \left\{\begin{matrix} r - r_0 \\ x_0 - x \end{matrix}\right\} \tag{6}$$

are introduced within the computational domain. Here, r_0 is the jet radius and x_0 is the axial location of the center of forcing. The forcing amplitude is given by $0 < \alpha \ll 1$ and the random variable (in time) $-1 \le \epsilon_i \le 1$. The phase ϕ_i is also updated randomly each time step. The index i denotes the azimuthal mode number with $i = 0$ being the axisymmetric mode and θ the azimuthal angle. LBL and UBL have adopted this forcing method as well. Note that $w' \equiv 0$. This method has been generalized to permit $w' \neq 0$ in [68]. This forcing is approximately nonradiating. Note also that the random update of ϵ_i in time will produce a space-time forcing that is not physically realizable, and the simulation will select those frequencies that it can support. What frequencies are kept is, in general, not known.

An alternative forcing scheme is to choose disturbances based on linear stability theory for a spatially evolving, parallel, annular mixing layer. In this approximation, the disturbances are expressed in a modal form (with implied real part)

$$q'(\boldsymbol{x}) = \sum_{m,n} \alpha_{mn} \hat{q}_{mn}(r) \exp[i(\omega_m t - k_{mn} x - n\theta + \psi_{mn})] \tag{7}$$

and the mean velocity $\langle \bar{u} \rangle$, mean density $\langle \bar{\rho} \rangle$, and mean speed of sound square $\langle \bar{a}^2 \rangle$ appear as coefficients in the compressible Rayleigh equation for the disturbance pressure

$$\frac{\mathrm{d}^2 \hat{p}}{\mathrm{d}r^2} + \left[\frac{1}{r} - \frac{1}{\langle \bar{\rho} \rangle}\frac{\mathrm{d}\langle \bar{\rho} \rangle}{\mathrm{d}r} + \frac{2k_{mn}}{(\omega_m - k_{mn}\langle \bar{u} \rangle)}\frac{\mathrm{d}\langle \bar{u} \rangle}{\mathrm{d}r}\right]\frac{\mathrm{d}\hat{p}}{\mathrm{d}r} + \left[\frac{(\omega_m - k_{mn}\langle \bar{u} \rangle)^2}{\langle \bar{a}^2 \rangle} - \frac{n^2}{r^2} - k_{mn}^2\right]\hat{p} = 0 \tag{8}$$

subject to the boundary conditions

$$|\hat{p}| < \infty \quad \text{as } r \to 0 \tag{9a}$$

$$\hat{p} \to 0 \quad \text{as } r \to \infty \tag{9b}$$

The far-field boundary condition ensures that the solutions obtained will be nonradiating. Equation (8) is an eigenvalue equation for the axial wave number k_{mn} for each real-valued frequency ω_m and azimuthal mode number n. When summed, the amplitudes are set by the user-chosen α_{mn} and the implied periodicity is broken by the

random walk variable ψ_{mn}. This method was used by ZFM for their Mach 0.9 jet and by BL for all of their jets. When the jets are supersonic, the boundary condition $\hat{p} \to 0$ will select only those instability modes that do not radiate to the acoustic far field, and will not permit supersonically convecting disturbances [69].

C. Far-Field Projection

Given a solution of the filtered, compressible Navier–Stokes equations, in principle, it is possible to include directly the "acoustic far field" with the turbulent near field in a single computational domain. Practically, however, such a calculation is beyond the computational resources currently available. Instead, it is common to use a projection technique wherein the midacoustic field is projected onto the true acoustic far field. The projection involves an assumption about how the sound propagates in the domain exterior to the LES calculation. In the available simulations, there appears to be three techniques that have been used in this regard. The first is a multiplication by $1/\mathcal{R}$, where $\mathcal{R}$ is the distance between a far-field observation point and the apparent source of emission of the observed sound on the jet centerline. The second, which was first used by Soh [70] and Lyrintzis and Mankbadi [71] for jet noise calculations, involves a Kirchhoff surface to solve the inviscid, linear wave equation in the exterior domain. The third method uses a Ffowcs Williams–Hawkings surface. Each method is described next.

1. *Multiplication by $\mathcal{R}^{-1}$*

Bogey et al. [14,17] use the geometric spherical spreading of $\mathcal{R}^{-1}$ to *estimate* the far-field radiated noise given the pressure data in the near to midacoustic field. The origin of the vector connecting the far-field point to the jet is arbitrarily defined as the apparent origin of the radiated sound and is not a fixed point within the jet. For example, at 90 deg from the downstream axis, the origin is taken slightly upstream of the potential core, whereas for sound radiated toward the 30 deg sector, the end of the potential core serves as the origin. The accuracy of this extrapolation is strongly dependent on the absence of hydrodynamic fluctuations present in the near-acoustic pressure signal. The hydrodynamic component, which naturally decays faster than $\mathcal{R}^{-1}$, will not be rejected by the geometric scaling. An example of the overprediction resulting from the multiplication of near- to midacoustic-field pressures by $\mathcal{R}^{-1}$ is given in Morris et al. [19].

2. *Kirchhoff Surface*

Under reasonable assumptions, the governing behavior of the acoustic disturbances may be accurately described by the linearized, inviscid wave equation. At the far-field distances commonly of interest ($100D_j$), the range of frequencies[¶] ($Sr = fD_j/U_j \leq 3$) and the amplitudes ($p_{\text{rms}}/p_\infty \leq 1 \times 10^{-3}$) expected in the simulations for the range of Mach numbers considered, viscous attenuation and nonlinear effects are minimal and may be neglected. The mean velocity and its gradient at far distances are sufficiently small so that their effect may too be ignored. The wave equation for pressure fluctuations $p' = \bar{p} - \langle \bar{p} \rangle$ about the mean pressure $\langle \bar{p} \rangle$ in a quiescent medium

$$(a_\infty^{-2}\partial^2/\partial t^2 - \partial^2/\partial x_j \partial x_j)p' = 0 \tag{10}$$

is thus appropriate for acoustic wave propagation. Under this idealization, the acoustic far field is related to the near field through a Kirchhoff surface [73,74] that encloses the jet. Pressure fluctuations on the surface of the cylinder are collected as functions of time and of the axial and azimuthal directions. The surface is chosen to be sufficiently far away from the nonlinear hydrodynamic region of jet so that the sound propagation is accurately described by the wave equation and extends from the computational inlet to the exit. The "ends" of the surface are not included as they do not lie in linear regions of the flow and thus the far-field sound predicted by the surface must be regarded as approximate. Freund et al. [75] developed a high-frequency approximation to reduce the error associated with using an open Kirchhoff surface, but it has not been adopted by the community.

There are two, equivalent methods that have been employed in solving Eq. (10) in the context of jet noise calculations. The first uses a statement of Green's theorem [76], where for a quantity that satisfies the wave equation, such as the pressure p', one may write

$$p'(\boldsymbol{x}, t) = \frac{1}{4\pi}\int_S \left[\frac{p'}{r^2}\frac{\partial r}{\partial n} - \frac{1}{r}\frac{\partial p'}{\partial n} + \frac{1}{a_\infty r}\frac{\partial r}{\partial n}\frac{\partial p'}{\partial t}\right](\boldsymbol{y}, t_r)\,\mathrm{d}^2\boldsymbol{y} \tag{11}$$

where $t_r = t - r/a_\infty$ is the retarded time and $r = |\boldsymbol{x} - \boldsymbol{y}|$ is the source-observer distance. S is the Kirchhoff surface and n is its outward-pointing normal. This form of the Kirchhoff representation was used by AED; ZFM used an equivalent form in the time-Fourier domain.

The second method, used by BL (and originally by Freund [15]), solves the wave equation in transformed coordinates for a Kirchhoff surface S defined as a right circular cylinder, of radius R_s, with generator along the jet axis. Using the pressure fluctuations specified on the surface S, the wave equation (10) is solved in the region exterior to S in the partially transformed form

$$\left(\frac{\mathrm{d}^2}{\mathrm{d}r^2} + \frac{1}{r}\frac{\mathrm{d}}{\mathrm{d}r} + \frac{\omega^2}{a_\infty^2} - k^2 - n^2/r^2\right)\hat{p} = 0 \tag{12}$$

which is also a limiting form of Eq. (8). Equation (12) is Bessel's equation and is subject to the boundary conditions that, for $r = R_s$, $\hat{p}_n(r; k, \omega) = \hat{P}_n(k, \omega)$ ($\hat{P}$ being the Fourier coefficient of p' measured on the Kirchhoff surface), and that as $r \to \infty$, the solutions represent outgoing traveling waves. Only those waves that satisfy $\omega^2/a_\infty^2 - k^2 > 0$ radiate as sound and contribute to the far field; closer to the jet, all modes will contribute. The far-field pressure fluctuations are found by integrating Eq. (12) to the desired value of r and inverse-transforming. The overall radiating solution at a given field point $\boldsymbol{x} = (x, r, \theta, t)$ is then seen to be

$$p'(\boldsymbol{x}, t) = \frac{1}{(2\pi)^2}\int^{+\infty}\int_{-\infty}\sum_{n=-N_\theta/2}^{N_\theta/2-1} \times \hat{P}_n(k, \omega)\frac{H_n^{(m)}(r\sqrt{\omega^2/a_\infty^2 - k^2})}{H_n^{(m)}(R_s\sqrt{\omega^2/a_\infty^2 - k^2})}e^{i(\omega t - kx - n\theta)}\,\mathrm{d}k\,\mathrm{d}\omega \tag{13}$$

where $H_n^{(m)}$ is the nth-order Hankel function. To enforce outgoing acoustic waves, one must take $m = 1$ for $\omega > 0$ and $m = 2$ for $\omega < 0$. The radial location R_s of the Kirchhoff surface is important to ensure that the nonlinearity and/or nonuniformities of the jet near field are sufficiently small to justify the assumptions made in the derivation. If the surface is placed too close to the near field, the far-field sound levels can be significantly overpredicted [77].

3. *Ffowcs Williams–Hawkings surface*

LBL, UBL, and SSS use the porous, stationary, Ffowcs Williams–Hawkings (Ff-H) surface [78] for the projection of the near to midacoustic field onto the acoustic far field. The Ff-H equation is a exact rearrangement of the governing equations of a compressible, viscous fluid in an integral representation; more details may be found in [79], for example. The end result is that the far-field pressure $p'(\boldsymbol{x}, t)$ can be expressed as the sum of three terms (whose names are derived from solid Ff-H surfaces)

$$p'(\boldsymbol{x}, t) = \underbrace{p'_T(\boldsymbol{x}, t)}_{\text{thickness}} + \underbrace{p'_L(\boldsymbol{x}, t)}_{\text{loading}} + \underbrace{p'_Q(\boldsymbol{x}, t)}_{\text{quadrupole}} \tag{14}$$

where, in the limit of $|\boldsymbol{x}| \to \infty$,

$$4\pi p'_T(\boldsymbol{x}, t) = \frac{1}{|\boldsymbol{x}|}\frac{1}{a_\infty^2}\frac{\partial}{\partial t}\int_S \{\ell_i \rho u_i\}(\boldsymbol{y}, t_r)\,\mathrm{d}^2\boldsymbol{y} \tag{15}$$

[¶]To estimate the laboratory equivalent, consider a Mach 0.9 isothermal jet with a 1 in. nozzle. $Sr = 2$ is approximately 22 kHz for which the atmospheric absorption [72] is 0.8 dB when the sound is measured at 100 diameters.

$$4\pi p'_L(\boldsymbol{x},t) = \frac{x_i}{|\boldsymbol{x}|^2}\frac{1}{a_\infty^3}\frac{\partial}{\partial t}\int_S \{\ell_i p + \ell_j \rho u_i u_j\}(\boldsymbol{y},t_r)\,\mathrm{d}^2\boldsymbol{y} \qquad (16)$$

$$4\pi p'_Q(\boldsymbol{x},t) = \frac{x_i x_j}{|\boldsymbol{x}|^3}\frac{1}{a_\infty^4}\frac{\partial^2}{\partial t^2}\int_{V_f} \{\rho u_i u_j + (p' - a_\infty^2\rho')\delta_{ij} - \tau_{ij}\}(\boldsymbol{y},t_r)\,\mathrm{d}^3\boldsymbol{y} \qquad (17)$$

and $t_r = t - |\boldsymbol{x}-\boldsymbol{y}|/a_\infty$ is the retarded, or emission, time, τ_{ij} is the viscous stress tensor, δ_{ij} is the Kronecker delta, ℓ_i is the unit outward-pointing normal of the surface S, and V_f is the volume of the fluid exterior to S.

The first two terms are associated with surface integrals involving monopolelike sources (for p'_T) and dipolelike sources (for p'_L). The third term p'_Q, which involves a volume integral of the fluid exterior to the surface, accounts for any sources outside the Ff-H surface. It is generally assumed in the calculations that all of the relevant noise sources are contained within the Ff-H surface so that the volume integral in p'_Q, which is computationally expensive to compute, is neglected.

The Ff-H surface approach has several advantages over the Kirchhoff surface approach described in the last section. By not being restricted to linear, inviscid wave propagation, the Ff-H surface can, in principle, be placed anywhere within the jet calculation, even in a nonlinear region of the flow where the Kirchhoff surface assumptions would be violated. This can result in a significant reduction in computational cost as a "tight" surface (in the sense of SSS) can be placed close to the jet and the overall computational domain can be smaller. Moreover, having a closer surface reduces the effects of numerical dispersion and dissipation on the wave propagation to the surface, especially for upwinded schemes. One must include the quadrupole term if important noise sources exist outside the Ff-H surface.

However, there is an open question as how to properly "close" the Ff-H surface in the nonlinear region of flow just as there is with the corresponding closure of the Kirchhoff surface. A more detailed discussion of this aspect of the Ff-H approach is given by Colonius and Lele [44] but the basic idea is as follows. The issue occurs when vortical motion passes through the surface and the quadrupole term p'_Q is neglected. Consider an inviscid vortex convecting at a constant subsonic speed that passes through the surface. Such a fluid motion does not generate sound. However, when the vortex passes through the surface, there is a nonzero contribution to the surface integrals represented by p'_T and p'_L that is exactly canceled by the volume integral of p'_Q. When the volume integral is neglected, this cancellation does not occur numerically and spurious noise is generated.

Various approaches have been formulated to address the problem; all are ad hoc and a completely satisfactory resolution remains to be found. UBL explored the effects of including or neglecting completely the closing surfaces and found a 3–4 dB difference between the two, with the closed surface being louder. They concluded, upon comparison with experimental data, that part of the overprediction of the far-field OASPL was caused by the closed surface evaluation, especially at low angles to the jet axis, i.e., $\Theta \leq 45$ deg. At a 60 deg angle, there was a minor difference ($\sim$0.5 dB) between the two approaches. Hence, UBL, and LBL also, use an open Ff-H surface.

SSS instead argue that a closed Ff-H surface is essential to properly predict the low-angle noise. In their method, they find that computing the far-field noise from a series of closed Ff-H surfaces, each with a different terminating location, x_{end} in their notation, and averaging yields the correct noise prediction. The argument for averaging follows from the observation that because the spurious noise is generated by the passing of vortical motions convecting at a low subsonic velocity through the outflow disk, the small size of the outflow disk does not effectively select the radiating components [32]. Thus, if one averages over an axial distance that is not small compared with a_∞/ω, the phase of the spurious noise can be canceled. They also note that the same effect could be obtained by averaging the raw pressure data $p'(\boldsymbol{x},t)$. Wang et al. [80] developed an approach to eliminate spurious noise in the calculation which includes the quadrupole noise. However, they considered only low-speed flows. SSS also modify the Ff-H formulation in Eqs. (15) and (16) when evaluating the noise from heated jets. They argue that the density on the outflow Ff-H surface should be replaced by the pressure assuming an isentropic relation, i.e., ρ becomes $\rho_\infty(p/p_\infty)^{1/\gamma}$.

III. Presentation of Data

In Table 1 are listed the jet operating conditions of the data to be presented in the following sections. Six different groups of operating conditions are present and include low- and high-speed jets, heated and unheated. The groupings result from the simulations of jets at conditions tabulated by Tanna [81], but the separation is not perfect. Thus, it was decided to group primarily on the basis of acoustic Mach number $M_a = U_j/a_\infty$ as this parameter is of fundamental importance, e.g., in the scaling of OASPL on U_j as derived by Lighthill [2]. Of next importance was the static temperature ratio, which is reported in the fourth column of Table 1. A "temperature scaling" similar to the dependence of the OASPL with U_j does not yet exist. Indeed, as found by Tanna [81], for jets with $M_a < 0.7$, heating increases the radiated sound whereas for those jets with $M_a > 0.7$, heating reduces the sound. Thus, T_j/T_∞ remains an important, and independent, parameter. This dependence has consequences when comparing jets at the same velocity but at different temperatures as no data collapse is yet possible.

In the final column of Table 1 is the jet Reynolds number, defined as $Re_D = \rho_j U_j D_j/\mu_j$, where the j subscript denotes evaluation at the jet exit. The Reynolds number range for a given set of U_j and T_j/T_∞ values can be considerable (often a factor of 20 and up to a factor of 100). It has been argued that for jet Reynolds numbers below 100,000 [82] or 400,000 [83] an independence of Reynolds number has not been reached. No explicit attempt has been made arrange the data according to the Reynolds number and, as will be shown, it does not appear that the Reynolds number is a controlling parameter in the data sets considered.

Numerical parameters for the simulations are likewise listed in Table 2 for each of the simulations (authors are listed in alphabetical order); only one listing is given for each independent set of simulations. The total number of points used in the simulation is given in the second column (denoted by N), whereas the effective azimuthal resolution is listed in the third. The second-to-last column is the momentum thickness δ_θ of the initial shear layers. In the case of SSS, the boundary-layer momentum thickness of $0.0036D_j$ is estimated to be two-thirds that of the initial shear layer momentum thickness once the boundary layers exit the nozzle. The data of Table 2 show that simulations with an order-of-magnitude difference in the number of points have been carried out. The azimuthal resolution also varies by an order-of-magnitude. In the next-to-last column, the subgrid scale (SGS) model used by the authors is listed, as discussed previously.

Note that in the presentation to follow, the axial coordinate has not been shifted to align the locations of the collapse of the potential core. Although many data are presented in a shifted fashion it was chosen to present the data in unshifted form. In simulations that do not have an explicit nozzle geometry, there is an ambiguity regarding the nozzle location and so there is arguable justification for an axial shift. For those calculations with a nozzle included, there is no such justification. It was chosen, therefore, to place all data on a common ground so as not to unnecessarily bias the discussion. Concentration is placed instead on the decay rates and peak values as these seem to be the more relevant quantities with respect to the acoustic far field.

A. Near-Field Data

Given the conditions laid out in Tables 1 and 2, the near-field data, presented using the mean centerline axial velocity U and its root mean square u_{rms}, are shown in Figs. 2–7. The data are organized

Table 2 Summary of the numerical parameters used

Authors	N, $\times 10^6$	$\Delta\theta$, deg	δ_θ/D_j	SGS[a]	Sr_a
Andersson et al. [30]	3.0	4.50	——	CSM	——
Bodony and Lele [35]	1.0	11.25	0.045	DSM	0.36
Bogey et al. [17]	6.1	1.73[b]	0.025	CSM	0.64
Bogey and Bailly [48]	12.5	3.00[b]	0.015, 0.025	EXP	1.07, 0.64
Lew et al. [41]	4.8	2.50[b]	0.045	EXP	0.36
Morris et al. [19]	1.0	10.00	——	DSM	——
Shur et al. [33]	1.2	5.63	0.005	IMP	3.20
Shur et al. [43]	3.0	2.25	0.005	IMP	3.20
Uzun et al. [39]	16.0	1.88[b]	0.025	DSM	0.64
Zhao et al. [18]	2.9	5.63	0.05	DSM, DMM	0.32

[a]. CSM denotes constant coefficient Smagorinsky SGS model; DSM denotes dynamic Smagorinsky SGS model; DMM denotes dynamic mixed model; EXP denotes explicit filtering for the SGS model; IMP denotes implicit numerical dissipation for the SGS model.
[b]. For the simulations with Cartesian grids (BBJ, UBL, and LBL) this value has been estimated from the number of points M contained within the range $0 < r \leq D_j/2$ as $\Delta\Theta \approx 360/(4 \times 2 \times M)$.

according to Table 1 in order of increasing jet Mach number. The data are presented normalized by the jet diameter D_j for the axial distance and by the jet velocity U_j for the axial velocity and its root mean square. In the groupings by acoustic Mach number, there may be some difference in U_j between the various simulations. It is known, see Lau [84] for example, that the mean velocity and axial fluctuations are weak functions of the jet velocity and temperature ratio. Within minor differences of U_j and T_j/T_∞, comparisons of velocity statistics of jets at different conditions are thus reasonable.

In Fig. 2 of the heated, $M_a = 0.5$ jets, the simulations of BL, LBL, and SSS are shown with the experimental data of Bridges and Wernet [85]. Recall that no axial shifting has been applied. All of the simulated data exhibit an earlier potential core collapse than the experimental data. The mean velocity decay rate is quicker for the simulation of BL than it is for that of LBL and SSS. For the fluctuations, the simulations of BL exhibit correspondingly higher levels compared with LBL simulations and a more rapid decay of $u_{\rm rms}$ with increasing axial position.

The velocity statistics for the unheated jets at the same jet velocity of $M_a = 0.5$ are shown in Fig. 3. The predicted length of the potential core is closer to the measured value. The simulations show different centerline velocity decay rates with the data of SSS being the closest to the experimental result. For the fluctuation levels, the data of BL peaks at a higher level than does the BB simulation. Both measurements of Ahuja et al. [86] and of Lau et al. [87] have roughly the same rate of growth of $u_{\rm rms}$ which is more closely predicted in the simulation of BB. Near $x = 0$, both simulations predict $u_{\rm rms} \to 0$, whereas the experiments exhibit some fluctuation.

Turning to the heated, acoustic Mach number 0.9 jets in Fig. 4, there is agreement in the potential core length among the simulations, but this value is shorter than what has been measured by Bridges and Wernet [85] and by Lau [84]. The rates of decay of the mean velocity of all of the simulations exhibit a qualitatively different behavior than what is measured. Whereas the measurements show an approximately linear trend in the range of $5 \leq x/D_j \leq 10$, especially for the more recent data, the simulation profiles are concave upward. That the measured data has some variation for $x/D_j \geq 10$ suggests there is some uncertainty for $x/D_j \leq 10$. The corresponding fluctuations shown in Fig. 4b demonstrate that the simulations of BL and LBL have higher predicted peak levels than do

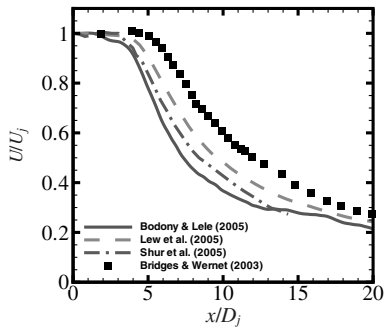

a) Mean centerline axial velocity, ■, Bridges & Wernet [84] ($M_a = 0.5$, $T_j/T_\infty = 1.76$)

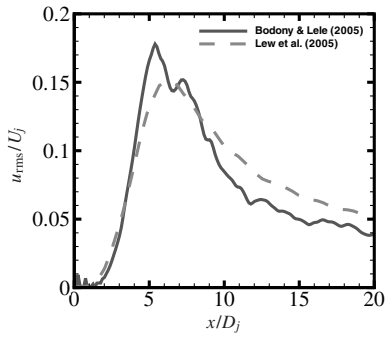

b) Centerline axial velocity root mean square

Fig. 2 Centerline axial velocity statistics for heated $M_a = 0.5$ jets. See Table 1 for conditions of the simulations.

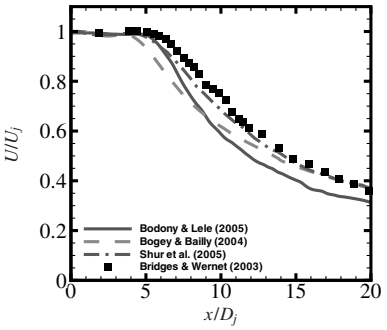

a) Mean centerline axial velocity, ■, Bridges & Wernet [84] ($M_a = 0.5$, $T_j/T_\infty = 0.95$)

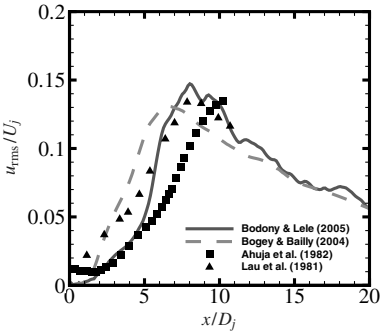

b) Centerline axial velocity root mean square, ■, Ahuja *et al.* ($M_a = 0.56$, $T_j/T_\infty = 0.97$);[85] ▲, Lau[83] ($M_a = 0.28$, $T_j/T_\infty = 1$)

Fig. 3 Centerline axial velocity statistics for unheated $M_a = 0.5$ jets. See Table 1 for conditions of the simulations.

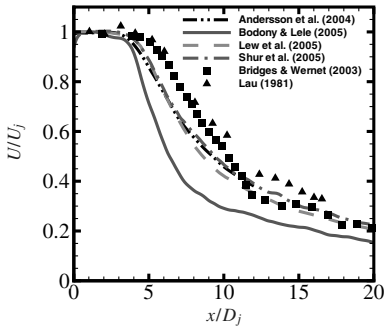

a) Mean centerline axial velocity, ■, Bridges & Wernet[84] ($M_a = 0.9$, $T_j/T_\infty = 2.7$); ▲, Lau[83] ($M_a = 0.76$, $T_j/T_\infty = 2.32$)

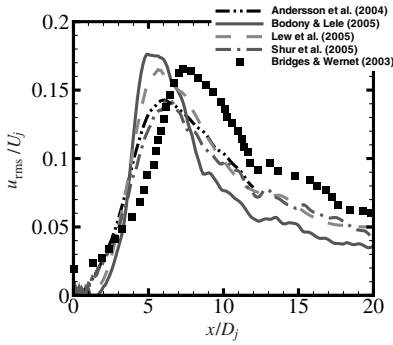

b) Centerline axial velocity root mean square, ■, Bridges & Wernet[84] ($M_a = 0.9$, $T_j/T_\infty = 2.7$)

Fig. 4 Centerline axial velocity statistics for heated $M_a = 0.9$ jets. See Table 1 for conditions of the simulations.

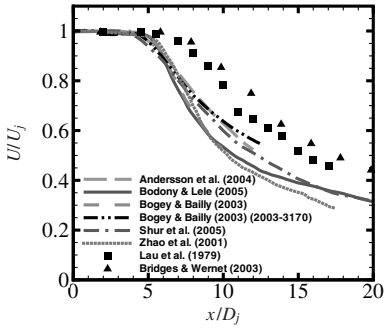

a) Mean centerline axial velocity, ■, Lau[86] *et al.* ($M_a = 0.9$, $T_j/T_\infty = 1$); ▲, Bridges & Wernet[84] ($M_a = 0.84$, $T_j/T_\infty = 0.86$)

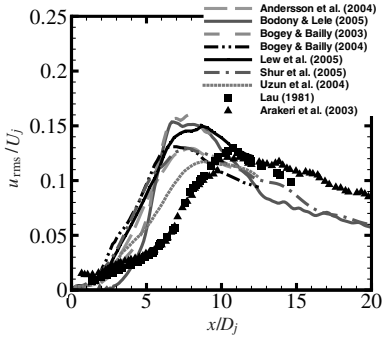

b) Centerline axial velocity root mean square, ■, Lau[84] ($M_a = 0.9$, $T_j/T_\infty = 1$); ▲, Arakeri *et al.*[104] ($M_a = 0.91$, $T_j/T_\infty = 0.97$)

Fig. 5 Centerline axial velocity statistics for unheated $M_a = 0.9$ jets. See Table 1 for conditions of the simulations.

the simulations of AED and SSS. LBL predict most closely the peak level of u_{rms} as measured by Bridges and Wernet [85].

As with their heated counterparts, the unheated $M_a = 0.9$ jets separate into two groups according their centerline velocity decay rates and peak fluctuation levels as shown in Fig. 5. The mean centerline velocity decay rate predicted by BL, BBJ, and ZFM is faster than that predicted by AED, BB, and SSS.

Figure 6 shows the mean centerline velocity and its root mean square for the heated $M_a = 1.5$ jet. Similar to the lower jet velocities, the mean velocity decay rate and the peak fluctuation levels of the BL simulation are higher than predicted by SSS. The authors are not aware of any corresponding experimental data against which to compare the simulations.

When the jet at the same velocity, but unheated, is considered in Fig. 7, the simulations of BL and MLSB have roughly the same peak fluctuation level which is slightly in excess of the experimental data. The centerline velocity decay rates, however, are not the same with the BL simulation being more rapid than measured by Lau et al. [87].

B. Far-Field Acoustic Data: Overall Sound Pressure Levels

In this section, the far-field overall sound pressure levels (OASPLs) are presented. The acoustic spectra will be shown later in Sec. III.C. Unlike the mean velocity and turbulence statistics, which have a weak dependence on the jet velocity U_j and static temperature ratio T_j/T_∞, the acoustic data are known to be stronger functions of these parameters. Only for the jet velocity does the OASPL have an established scaling law which can be used for data reduction; the static temperature ratio remains an independent, and important, parameter. Following standard procedure (see, e.g., Ahuja [88]), the OASPL is scaled to a distance of $100D_j$ and to the particular value of M_a under consideration according to

$$\text{OASPL}_{\text{scaled}} = \text{OASPL}_{\text{reported}} - 20\log_{10}\frac{100D_j}{\mathcal{R}_{\text{reported}}} + 80\log_{10}\frac{M_a}{M_{a,\text{reported}}} \quad (18)$$

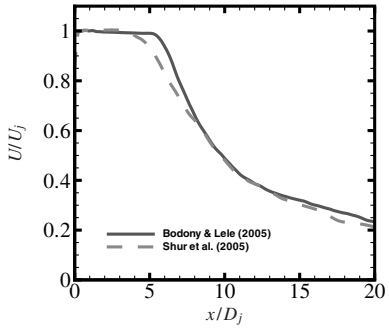

a) Mean centerline axial velocity

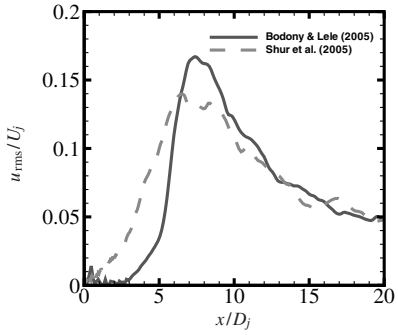

b) Centerline axial velocity root mean square

Fig. 6 Centerline axial velocity statistics for heated $M_a = 1.5$ jets. See Table 1 for conditions of the simulations.

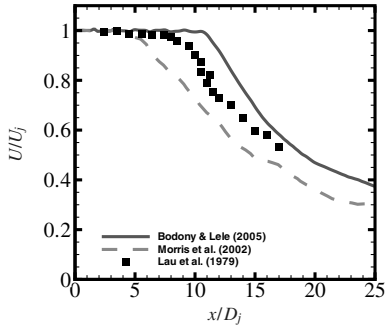

a) Mean centerline axial velocity, ■, Lau *et al.* [86] ($M_a = 1.37$, $T_j/T_\infty = 1$)

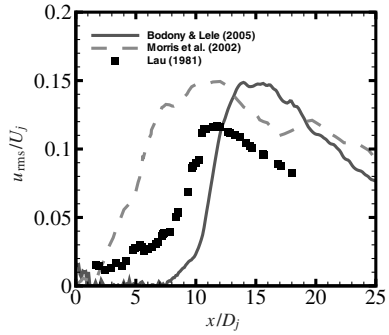

b) Centerline axial velocity root mean square, ■, Lau [83] ($M_a = 1.37$, $T_j/T_\infty = 1$)

Fig. 7 Centerline axial velocity statistics for unheated $M_a = 1.5$ jets. See Table 1 for conditions of the simulations.

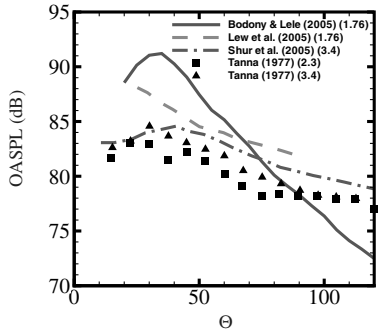

a) Heated jet, ■, Tanna[80] ($M_a = 0.5$, $T_j/T_\infty = 1.76$); ▲, Tanna[80] ($M_a = 0.5$, $T_j/T_\infty = 3.4$)

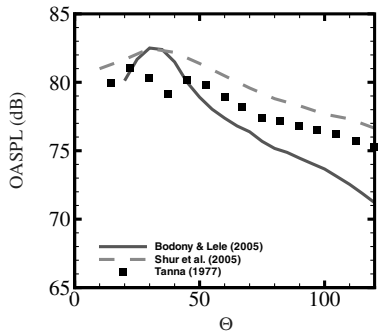

b) Unheated jet, ■, Tanna[80] ($M_a = 0.5$, $T_j/T_\infty = 0.95$)

Fig. 8 Far-field OASPL for $M_a = 0.5$ jets. See Table 1 for conditions of the simulations.

This scaling has been applied equally to heated and unheated jets, although there is some open discussion regarding the U_j^8 relation for heated jets [89].

The heated $M_a = 0.5$ jet is shown in Fig. 8a for two static temperature ratios: BL and LBL at $T_j/T_\infty = 1.76$ and SSS at $T_j/T_\infty = 3.4$. There are experimental data taken by Tanna [81] for each of the temperature ratios. For the lower temperature jet, both predicted OASPL are 5–8 decibels (dB) above the measured values. The sound is much more directed toward $\Theta = 40$ deg in the simulation by BL. LBL, in contrast, more uniformly overpredict the Tanna data [81]. At the higher temperature ratio, the SSS prediction is closer to 1–2 dB over the Tanna measurements at angles $\Theta >$ 40 deg and commensurate at lower angles. There is a 10 deg shift in the peak OASPL for the BL and SSS simulations relative to Tanna's data [81].

At the unheated condition in Fig. 8b, there is closer agreement between the simulations of BL and SSS for the peak radiation, but systematic differences remain. Both simulations have the same peak directivity angle of $\Theta = 30$ deg and the same sound level at that angle but differ greatly in their directivity. SSS are consistently 1.5 dB above Tanna's data [81], whereas BL predict a more sharply directive sound field.

In Fig. 9a, the heated $M_a = 0.9$ jets are shown from simulations of AED ($M_a = 0.75$ and $T_j/T_\infty = 2$), BL and LBL at $M_a = 0.9$ and $T_j/T_\infty = 2.7$, and of SSS at $M_a = 0.9$ and $T_j/T_\infty = 3.4$. The data of Tanna [81] at the same conditions as the SSS simulation are also given; at this Mach number, the change in OASPL between static temperature ratio of 2.7 and 3.4 is minor, and so only the higher temperature ratio is shown. The BL simulation overpredicts the peak OASPL value by 4–5 dB, whereas SSS are quieter by about 2–3 dB at peak. The SSS simulation agrees with the measurements at larger angles of $\Theta > 50$ deg. The simulations of BL, LBL, and SSS overpredict the peak radiation angle by approximately 10 deg.

For the unheated jet at acoustic Mach number of 0.9, the simulation data are shown in Fig. 9b with the experimental data of Tanna [81] and of Viswanathan [83]. At the peak radiation direction, there is an approximate 3 dB scatter among the simulations and about 1 dB within the measurements. The simulated data show an increased amount of scatter at larger angles whereas the measurements exhibit less variance. The predictions of BL and Bailly et al., which well predict the low-Reynolds-number jet of Stromberg et al. [16], overpredict the higher Reynolds number data of Tanna [81] and Viswanathan [83] at low angles and underpredict at larger observer angles. The simulations of SSS and UBL more closely follow the experimental data at larger angles.

The high-speed, heated jet ($M_a = 1.5$ and $T_j/T_\infty = 2.3$) OASPL predictions are shown in Fig. 10a. The data of SSS are at a slightly higher temperature ratio $T_j/T_\infty = 2.67$. The predictions of BL agree well with the data of Tanna [81] and of Viswanathan [83] for angles $\Theta \leq 100$ deg with underprediction at large angles. The data of SSS have a less directive distribution and are 2–3 dB above the measurements.

The unheated $M_a = 1.5$ jet is shown in Fig. 10b. Note that the data of SSS in this figure is of an isothermal jet ($T_j/T_\infty = 1$), whereas the "cold" jet has $T_j/T_\infty = 0.56$. This difference is important and one cannot directly compare the two simulations. The data of BL and the measurements of Tanna [81] are, however, at the same condition and predictions agree with the measurements to within 1 dB for angles less than 100 deg. The SSS predicted directivity is more uniform than that found by BL and by MLSB, similar to the data of Fig. 10a.

C. Far-Field Acoustic Data: Spectra

In this section, the acoustic spectra data are presented. It is common for acoustic spectra to be reported in the literature in one-third-octave and in narrowband form. Direct comparison of one-third-octave spectra to narrowband spectra is not necessarily valid given the increasing bin averaging width used in one-third-octave data with increasing frequency. Hence, it was chosen to present one-third-octave solely, especially because most of the available data exist in this form.

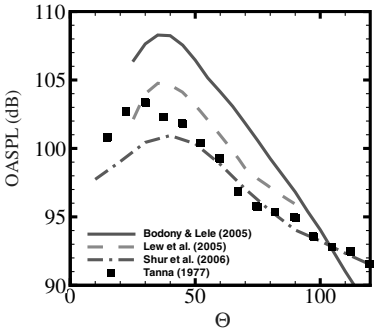

a) Heated jet, ■, Tanna[80] ($M_a = 0.9$, $T_j/T_\infty = 3.40$)

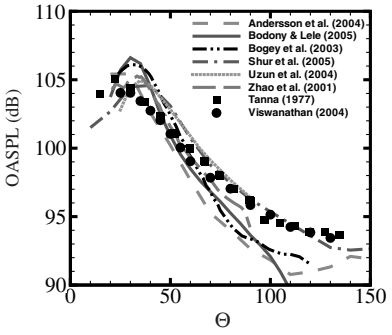

b) Unheated jet, ■, Tanna[80] ($M = 0.9$, $T_j/T_\infty = 0.84$);
●, Viswanathan[82] ($M_a = 0.84$, $T_j/T_\infty = 0.86$)

Fig. 9 Far-field OASPL for $M_a = 0.9$ jets. See Table 1 for conditions of the simulations.

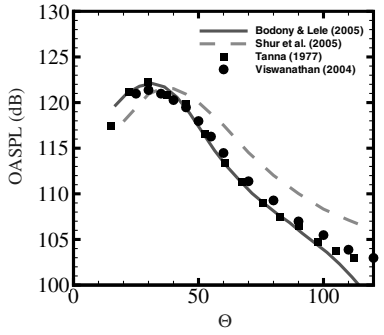

a) Heated jet, ■, Tanna[80] ($M_a = 1.5$, $T_j/T_\infty = 2.3$)
●, Viswanathan[82] ($M_a = 1.5$, $T_j/T_\infty = 2.75$)

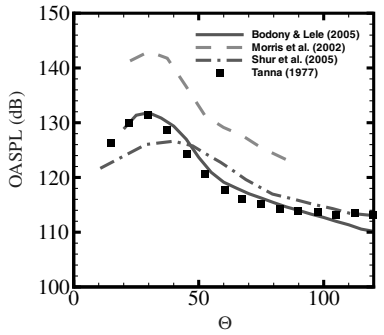

b) Unheated jet, ■, Tanna[80] ($M_a = 1.5$, $T_j/T_\infty = 0.56$)

Fig. 10 Far-field OASPL for $M_a = 1.5$ jets. See Table 1 for conditions of the simulations.

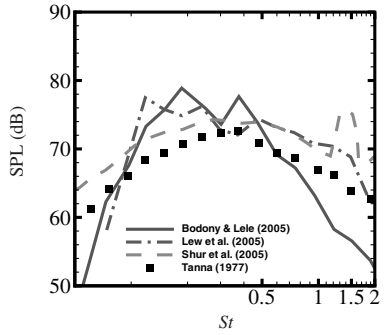

a) Heated jet, ■, Tanna[80] ($M_a = 0.5$, $T_j/T_\infty = 2.30$)

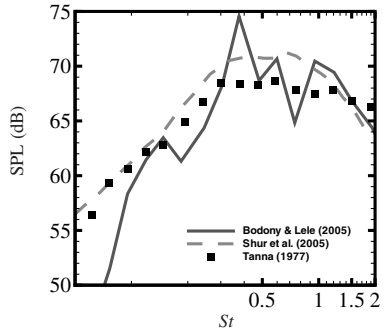

b) Unheated jet, ■, Tanna[80] ($M_a = 0.5$, $T_j/T_\infty = 0.95$)

Fig. 11 Far-field acoustic spectra for $M_a = 0.5$ jet at $\Theta = 45°$ and $100D_j$.[**]

The spectra at $\Theta = 45$ deg for the subsonic simulations of BL, LBL[**], and SSS are given in Figs. 11a, 11b, 12a, and 12b in comparison with selected spectra from Tanna [81]. The data are presented in one-third-octave form at a common distance of $100D_j$.

For the Mach 0.5 jets shown in Fig. 11, the spectra of BL peak, on average, at a lower frequency than those of SSS. For the heated Mach 0.5 jet, as might be expected from the OASPL at this condition given in Fig. 8a, the predicted spectra of BL overpredicts the sound pressure levels (SPL). The SSS data mildly overpredict the spectral levels nearly uniformly with frequency. The large oscillations in the spectra of BL and LBL at low frequencies suggests insufficient statistical sample. The SSS data have an anomalous increase in the heat jet spectrum near $Sr = 1.5$.

Similar observations hold for the $M_a = 0.9$ jets of Fig. 12, though with improved statistical sample. For the heated jet, the SSS data more closely agree with the measured spectrum of Tanna [81]. At the unheated condition, the BL spectrum has a lower peak frequency than does the SSS spectrum. The corresponding unheated Mach 0.9 far-field spectra of BBJ are given in Fig. 13.

IV. Discussion

The near- and far-field data presented in the previous section demonstrate that the relationship between the jet operating conditions, e.g., heated vs unheated, etc., the jet mean velocity and fluctuation levels, and the acoustic field are captured *qualitatively* by the simulations. Within the set of simulations by AED, BL, LBL, and SSS, the predictions show an increase in sound levels with heating for jets with $M_a < 0.7$ and a decrease in sound levels with heating for jets with $M_a > 0.7$. In general, the peak turbulence levels decrease with increasing jet Mach number and increase with heating (at constant U_j), in accordance with measurements (see, e.g., Lau [84]). In this section, the discussion focuses on the quantitative scatter in the predictions to determine potential underlying causes.

[**]The one-third-octave spectra shown in [41] for the subsonic heated jets are in error. The spectra shown in Figs. 11 and 12 were given to the authors directly by Mr. Lew. The OASPL values in the aforementioned reference are correct.

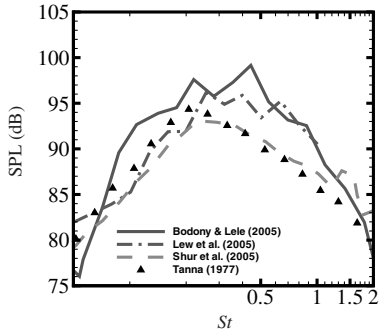

a) Heated jet, ■, Tanna[80] ($M_a = 0.9$, $T_j/T_\infty = 3.40$)

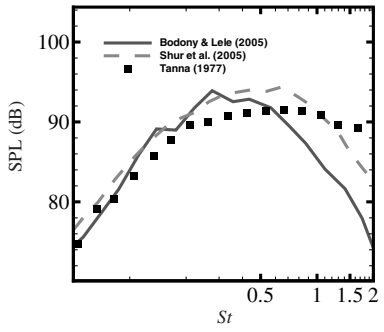

b) Unheated jet, ■, Tanna[80] ($M_a = 0.9$, $T_j/T_\infty = 1.00$)

Fig. 12 Far-field acoustic spectra for $M_a = 0.9$ jet at $\Theta = 45°$ and $100D_j$.[**]

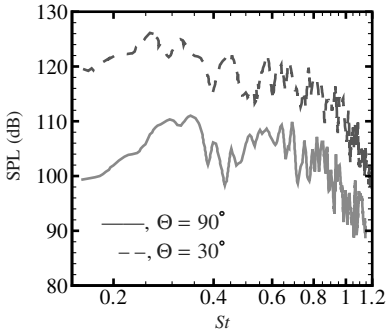

Fig. 13 Narrowband spectra at $\Theta = 30$ and 90 deg for the unheated Mach 0.9 jet of BBJ. Data presented at $100D_j$.

To this end, there have been previous studies by Andersson et al. [30], Bodony and Lele [20], Bogey and Bailly [22], Lew et al. [40], and Morris et al. [19] that explored the effects of 1) inflow forcing, 2) initial shear layer thickness, and 3) subgrid scale model choices on the radiated sound. Andersson et al. [30] and Bogey and Bailly [25] additionally considered 4) the dependence on the Reynolds number. These parameters are discussed separately.

A. Influence of Inflow Forcing

It is acknowledged in each of the simulations that the inflow forcing, or its absence, has a direct impact on the predicted mean velocity, its level of fluctuations, and on the radiated sound. The particular choices made by the authors were discussed earlier in Sec. II.B.2 where three primary methods were mentioned. In no particular order, the methods are 1) no explicit forcing, 2) vortex ring forcing, and 3) eigenmode forcing. Each of these methods aims to induce a natural development of the turbulence within in the early, relatively thin, annular shear layers in such a way that the downstream properties of the jet are consistent with experimental data. Most notably, the mean velocity decay rate and the peak level of u_{rms} are consistently used as metrics in this regard. Although other properties may be considered, u_{rms} has been the most commonly reported.

For a given nozzle geometry, method 1 has, as noted by SSS, no adjustable parameters once the boundary layer profile is chosen and is, of course, the simplest to implement. It is argued, as done by SSS, that in an experimental setting, no explicit forcing is applied to the jet and this situation should be reproduced in the simulation. This approach neglects any unsteadiness that may be present within the nozzle upstream of the exit produced by the upstream piping. As noted by Viswanathan and Clark [90], the internal nozzle geometry can influence the radiated sound through modification of the nozzle boundary layer at the nozzle exit. Both the thickness and the fluctuation level (laminar, quasi laminar, or fully turbulent) are found to modulate the radiated noise spectrum, especially for heated jets. Andersson et al. [30] noted little change in OASPL near $45 \leq \Theta \leq 110$ deg when synthesized turbulence is added upstream of the nozzle exit and a more directive sound field, with changes on the order of 1 dB around 30 deg, when a specified nozzle inlet boundary layer profile was used. (The changes are relative to uniform inlet conditions without imposed disturbances.) That the nozzle geometry plays a central role in the generation of shear layer disturbances via a scattering process, the nozzle-lip geometry is likely to be important.

For methods 2 and 3, which explicitly inject disturbances into the initial shear layers, experimental data [86,91] suggest there exists a link between the azimuthal coherence of the disturbance modes to the overall jet development. Those studies find that the azimuthally coherent [$n = 0$ in Eq. (8)] mode can adversely enhance the turbulence levels above nonforced jets with a resulting increase in the sound radiation. Numerically, these effects have been found by Morris et al. [19] and by Bodony and Lele [20]. Consequently, simulations using eigenmode forcing do not explicitly force the azimuthal mode. Those studies using the vortex ring method 2, in contrast, have found less sensitivity to the presence of the axisymmetric mode. Lew et al. [40] note an axial shifting of the jet as lower-order modes are removed but with a roughly constant peak turbulence level. Bogey and Bailly [22], on the other hand, witness a reduction in the peak centerline turbulence levels when the lower azimuthal modes are dropped and a reduction of the OASPL in the near-acoustic field. (Far-field OASPL data were not given by Bogey and Bailly [22].)

The forcing amplitude used in methods 2 and 3 can also have a direct effect on the radiated sound. For a constant shear layer thickness, Bogey and Bailly [22] report that decreasing the amplitude by one-half results in an increased centerline fluctuation level and an increased near-field OASPL for an unheated Mach 0.9. Bodony [92] found, on the other hand, a large decrease in the turbulence levels and radiated sound for a Mach 0.5 unheated jet was observed when the amplitude was decreased by 40%. For a Mach 0.5 heated jet, Bodony [92] found very little dependence of the turbulence and in the radiated sound to the forcing amplitude. At the higher velocity of $M_a = 1.5$ the unheated jet of BL also exhibited little dependence on changing the forcing amplitude by 50% (see Fig. 14).

B. Influence of the Initial Shear Layer Thickness

It is known that resource limitations have thus far required an artificial increase in the initial shear layer thickness used in the simulations relative to values more typically found in experimental jets. The distribution of initial momentum thicknesses found in the present survey is given in Table 2 in which a typical order of magnitude is $\delta_\theta/D_j \sim 10^{-2}$; values closer to 10^{-3} are generally found experimentally [90]. The precise cause-and-effect of thicker shear layers on the turbulence and radiated sound has not been characterized experimentally and only the study of Bogey and Bailly [22] has attempted a numerical characterization.[††] In their study, BB find that decreasing the initial shear thickness reduces the centerline mean velocity decay rate, the fluctuation levels, and the near-field OASPL. Indeed, among those simulations that are listed in Tables 1

[††]Kim and Choi [5] have examined the relationship between the initial shear layer thickness and jet development for incompressible jets.

and 2, the OASPL predictions in Fig. 9b for the $M_a = 0.9$ unheated jet, which has received the most attention, generally follows the trend of decreasing peak OASPL with decreasing initial shear layer thickness. A similar correlation in the axial velocity fluctuation levels may be found in Fig. 5b. The axial velocity statistics for all other conditions also exhibit this trend.

Further evidence of this may be found in the temporal turbulence spectra along the jet lip line in Figs. 15–17 for the simulations of BL, BBJ, and SSS, respectively. In the simulations of BL and BBJ, which have thicker initial shear layers relative to SSS, the temporal spectra are biased toward the lower frequencies at locations near the nozzle exit. The data of SSS are, in contrast, more heavily weighted toward frequencies above $Sr = 1$. As the turbulence within the jets develops, these spectra become more broadband in nature. From inviscid stability estimates, it is known that thinner shear layers support higher frequencies [93]. Based on the data available, it appears that having thinner initial shear layers is to be preferred in the overall predictive accuracy of the turbulence and the sound levels.

C. Interrelationship Between the Shear Layer Thickness and the Inflow Forcing

The two preceding subsections are not independent, and it is important to discuss them in this regard. The studies of Crow and Champagne [91] and of Ahuja et al. [86] focused on the response of axially symmetric jets to imposed acoustic disturbances. Their two primary findings were that 1) the jet is a "selective amplifier" [91] for instability modes with frequencies around $Sr = 0.3$, and 2) that forced jets generally are louder with increased fluctuation levels and a more rapid centerline decay of the axial velocity. The modes responsible for item 1 are the so-called jet column modes, whose spatial properties are dependent on the entire jet structure, having axial wavelengths on the order of the jet diameter. Ahuja et al. [86] showed that high-speed jets exhibited qualitatively similar behavior to the incompressible jets, even when heated.

It is also well known that annular shear layers support a distribution of spatial instability modes, such as were used in Eq. (8). For frequencies up to $\omega\delta_\theta/U_j = 0.2$–$0.3$, depending on the flow condition, the modes are unstable with the peak amplification for the axisymmetric mode occurring at $\omega\delta_\theta/U_j = 0.1$ [93]. In terms of Strouhal number, this peak corresponds to $Sr_a(\delta_\theta/D_j) = 0.016$. Using the values of δ_θ/D_j in Table 2, one is able to find the most amplified Strouhal number Sr_a based on the initial shear layer thickness for each of the simulations. These values are listed in the last column of Table 2.

Those simulations with initial shear layer thicknesses $\delta_\theta/D_j \gtrsim 0.03$ thus support instability modes in the initial shear layers that are very close to the most preferred mode of the jet, suggesting that the early regions of those jets will have significant jet column mode dynamics. These jets will not be of the "tone-forced" quality explored by Crow and Champagne [91] and by Ahuja et al. [86], but will have some of the same characteristics, including a faster centerline decay rate of the axial velocity and higher levels of the axial velocity fluctuations. By explicitly forcing the initial shear layers at frequencies near $Sr_a \approx 0.3$, the jet vigorously responds with increased fluctuation levels and increased values of the OASPL. As case in point, consider Fig. 5b for the centerline axial u_{rms} distribution. The simulations of BL ($Sr_a = 0.36$), BBJ ($Sr_a = 0.64$), and LBL ($Sr_a = 0.32$) show the largest peak value of the fluctuating velocity. In the far-field directivity of the same jet (Fig. 9b), the BL and BBJ simulations exhibit larger OASPL levels by 1–1.5 dB. (LBL did not report OASPL for this case.)

Conversely, simulations with thin initial shear layers, particularly those of SSS, will selectively amplify instability modes with $Sr_a \gg 0.3$ whose characteristics will be weakly dependent on D_j and well approximated by the local *planar* shear layer dispersion relation. As the near-nozzle shear layer is most receptive to external disturbances whose wavelengths are on the order of the local thickness, the nozzle will preferentially generate, due to scattering, those disturbances with $Sr \gg 0.3$ and likely not acquire a tone-forced quality.

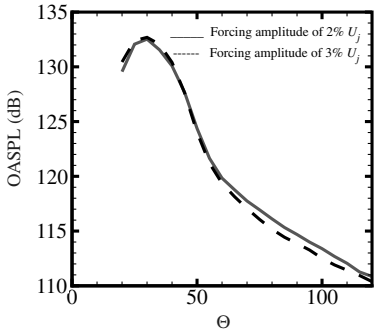

Fig. 14 Forcing sensitivity of $M_a = 1.5$, unheated jet of BL.

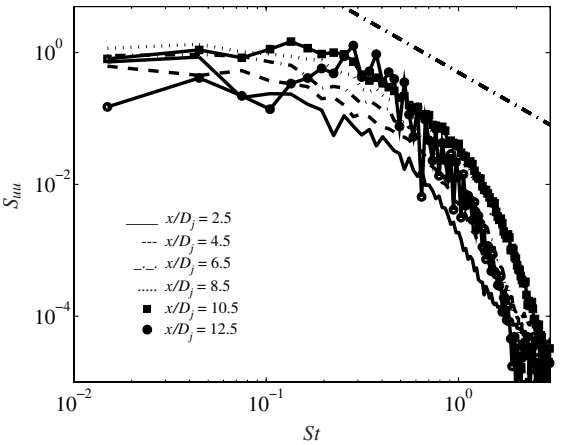

Fig. 15 Temporal spectra S_{uu} of u' for the Mach 0.9, unheated jet of BL taken on $r/D_j = 0.5$.

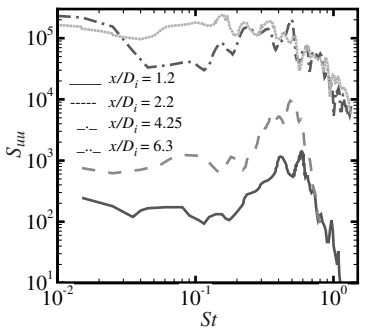

Fig. 16 Temporal spectra S_{uu} of u' for the Mach 0.9, unheated jet of BBJ taken on $r/D_j = 0.5$.

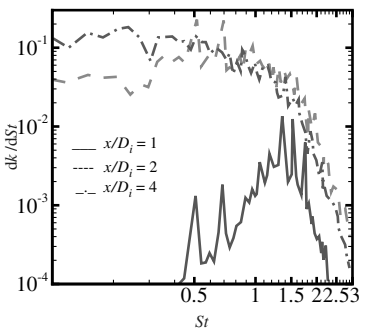

Fig. 17 Spectra at resolved turbulent kinetic energy at $r/D_j = 0.45$ for Mach 0.9 isothermal jet of SSS.

D. Influence of the Subgrid Scale Model

The relationship of the subgrid model used in the LES, if one is used at all, to the quality of the jet LES predictions has received some attention but no consensus exists. In the context of wall-bounded turbulence, the issue of the SGS model effects on transition has received significant attention, with particular emphasis placed on the models' effective dissipation. For jet noise, the information is much less mature and primarily consists of one-off tests comparing results with and without SGS models. This section highlights all of the studies known to the authors whose purpose was to elucidate the role the SGS model plays in the prediction quality.

Andersson et al. [30] found a minor dependence in their far-field OASPL with changes in the subgrid model but a more dramatic change when the model length scale $\Delta = (\Delta x \Delta y \Delta z)^{1/3}$ is increased to $\sqrt{2}\Delta$, effectively increasing the subgrid viscosity. In the latter change, the centerline axial velocity decreases but the near-field turbulence levels increase, becoming closer to the measured values in magnitude, but shifted downstream. The far-field OASPL increases with the increased filter width and overpredicts the measurements. Note that AED's Fig. 6 is qualitatively similar to Shur et al.'s Fig. 4 in [32].

Bogey and Bailly [94] cite a "decreased effective Reynolds number," with reduced turbulence and noise levels, when the dynamic Smagorinsky model is used relative to an explicitly filtered calculation. Similar to Bodony [92], they note an increase in the local mean velocity when the SGS model is turned off. They observe a decrease in the centerline axial velocity fluctuations along the jet centerline, however, when the model is turned off. In the acoustic near field, removing the SGS model increases the energy in the pressure fluctuations above $Sr = 0.3$ for their observation location, implying an increase in the local OASPL.

Uzun et al. [95] conclude that the near-field turbulence levels are sensitive to the choice of constants when using a constant coefficient Smagorinsky model and infer, but do not demonstrate, a sensitivity to the far-field sound as well. Recently, Uzun et al. [96] have quantified the dependence of the far-field sound on the presence or absence of the SGS model in their formulation. They find that the noise for frequencies less than $Sr \approx 1$ is increased when using the dynamic Smagorinsky model relative to a simulation using only selective filtering. As their jet appears to be too loud compared with the measured data by Tanna at all angles, they speculate that for angles closer to the jet axis the OASPL predicted with the SGS model are more accurate, whereas at larger angles the nonmodel predictions are preferred.

Zhao et al. [18] find that the dynamic Smagorinsky model yields lower turbulence and far-field OASPLs (on the order of 2–3 dB) relative to the dynamic mixed model. (The latter model is often considered less dissipative than the former model [52].)

For those groups who have reported cases both with and without an SGS model, the data support the view that their results are sensitive to the SGS model used, including the absence of the model. The details of the sensitivity appear to be dependent on the particular implementation for most quantities; the exceptions being 1) the decrease in the local mean velocity when a model is used and 2) the increase in the higher frequencies of the sound spectra when a model is absent. It is interesting that BB find larger fluctuations levels on the jet centerline when an SGS model is present, although BL do not. ZFM also report a reduction in the turbulence levels when a more dissipative model is used.

E. Influence of the Reynolds number

The studies of Andersson et al. [30] and Bogey and Bailly [25] explicitly considered the effect the jet Reynolds number plays in the near- and far-field predictions. In the Andersson et al. [30] study, the Reynolds number for the unheated $M_a = 0.75$ was increased from 50,000 to 900,000, with the higher number being the same as measured in a corresponding experiment. When increased by more than an order-of-magnitude, very little change was observed in the turbulence levels and in the radiated sound. Note that their study used wall functions around the nozzle.

Bogey and Bailly [25] systematically varied the Reynolds number of their Mach 0.9 unheated jet between 1700 and 400,000. See also their more recent work in [97]. With decreasing Reynolds number, they find an increasingly low-frequency biased near-field acoustic spectrum, with a corresponding shift in the near-field OASPL, but observed little change in the peak OASPL. For Reynolds numbers between 10,000 and 400,000, the viscous dissipation becomes a negligible part of the energy budget, but a more precise estimate of the transition from viscous-to-SGS model dissipation is not yet available.

If the data of Fig. 9b are considered it appears, consistent with the two aforementioned studies, the jet Reynolds number is not a primary parameter in the simulations in explaining the difference between predictions at approximately the same conditions. Indeed, one cannot find a consistent variation of the far-field sound levels with Reynolds number for jets at the same Mach number and temperature ratio. In light of Bogey and Bailly's findings [97], it might have been expected that Andersson et al. [30] saw little change for the latter study's change in Reynolds number. (It is here not meant that the Reynolds number is unimportant to the structure of the radiated sound field; the systematic variation of Re_D in the studies of Bogey and Bailly [25,97] clearly demonstrates its relevance.) It appears that the shear layer properties are more important at the current level of simulation fidelity. It is likely that as thinner initial shear layers are considered, the simulation Reynolds number will become more relevant.

F. Limitations of the Current Paper

We conclude this discussion by explicitly mentioning the limitations inherent in this paper. Because of the limited amount of data available, specifically in the limited number of studies conducted using the same physical conditions, we found it necessary to supplement the available data with physical reasoning and scaling arguments. This was especially true in Secs. IV.C and IV.D which looked at the effects of the inflow forcing and shear layer thickness. As more studies are published, it will be important to critically revisit our conclusions in light of the additional data.

V. Comments on the State of the Art and Future Directions

Since 2000, there has been significant effort by the community to improve the predictive quality of large-eddy simulation for jet noise. Unfortunately, the research has been done in a largely ad hoc manner by the community such that one cannot say which numerical approach is preferred. For example, the role the SGS model plays cannot be completely quantified as, depending on the study, including the model either increases or decreases the near-field turbulence levels relative to leaving it out. During the revision of this paper, the paper by Wang et al. [1] appeared and presents these and other open issues in the broader context of computational aeroacoustics. The reader is referred therein for additional discussion.

A. Key Open Issues

What is clear are the following two key points, which encompass the outstanding issues remaining in the physical modeling of jet noise prediction.

1) The use of an SGS model or absence of one in favor of a high-wave number filter or dissipative numerics has a strong influence on the predictions. Although it is clear that using a subgrid scale model adds diffusivity to the simulations, it has not been established that it is improper to do so. The history of large-eddy simulation in other flows suggests that the sensitivity of the transition process to the dissipation added by the subgrid scale model is the mechanism by which the model's influence is felt. However, as noted by Bogey and Bailly [97], the total dissipation added by the model (or filtering in their case) is a strong function of the Reynolds number. Thus, the model also acts cumulatively on the dynamics of the jet flow.

2) The influence of the inflow conditions cannot be understated. For the data reviewed in this paper, this influence, in particular that due to the thickness of the initial shear layers, appears as the dominant parameter in determining the accuracy of the prediction, keeping in mind the sensitivity of the predictions to the SGS model used. The thinner the initial shear layer, insofar as it is comparable to the experimentally observed values, the more accurate the prediction of the near-field turbulence and the far-field sound. This assessment assumes that the simulations are sufficiently resolved to support the thin shear layers with numerics that are not overly dissipative.

The two issues specific to the inflow conditions, apart from the thickness of the initial shear layers, are 1) nozzle geometry and 2) imposed forcing. It is our view that including the nozzle geometry is the preferred method. Imposing an initial velocity profile does work for certain cases but introduces a series of parameters that the user must specify. Higher speed jets appear to be less sensitive to these parameters than are low-speed (especially heated) jets. However, the recent attempt by Uzun and Hussaini [98] shows that including nozzle does not guarantee excellent agreement with experiment. The results of Barré et al. [99] suggest that turbulent nozzle exit boundary layers may indeed yield lower far-field noise levels relative to jets with laminar exit boundary layers.

B. Predictive State of the Art

Within the uncertainty associated with the role of the SGS model and of the inflow boundary conditions, the predictive capability of large-eddy simulation for *moderate to high-speed jets* is as follows:

1) The potential core length is not accurately predicted due to the uncertainty regarding the inflow conditions, especially for those simulations that model the nozzle geometry with specified inflow conditions.

2) Using a shifted axial scale, the centerline quantities U and u_{rms} are predicted within the apparent experimental uncertainty *when* the appropriate inflow conditions are used. When the inflow shear layers are too thick, the centerline velocity decay is too rapid and the peak value of u_{rms} is too high. There is insufficient data presented in the literature to comment on other quantities.

3) The far-field OASPL (directivity) is more uncertain than the near-field quantities due to the issue of how to properly project the far-field sound using open, rather than closed, Kirchhoff and Ff-H surfaces. At this stage, it appears that an uncertainty of ± 2 dB exists in the ability of LES to accurately predict the sound from high-speed jets. At lower speeds, the uncertainty greatly increases.

4) Of particular concern to industry is the Strouhal number limit of the LES predictions due to resource, and hence resolution, limitations. At present, we are capable of predicting frequencies up to $Sr \approx 1.5$–3.0, depending on the flow condition. To be more useful to frequency-weighted measurements, we need to get to Strouhal numbers closer to eight.

C. Future Directions

Considering the future of large-eddy simulation with respect to jet noise predictions, several points of interest are apparent. These items are itemized next in order of decreasing importance.

1) Role of the SGS model: At present this feature of LES predictions of jet noise is the most outstanding. Although numerous groups have compared their predictions with and without SGS models, a clear picture has not yet developed just how the SGS model correctly or incorrectly models the relevant physical processes and how it interacts with the numerics. To decipher the role of the SGS model, a series of numerical experiments needs to be conducted wherein the influence of numerical dissipation and grid resolution are quantified. For these studies to be useful, the far-field sound must be computed, not estimated using a geometric scaling.

2) Proper inclusion the nozzle geometry: The works of Uzun and Hussaini [98] and Barré et al. [99] are suggestive that a detailed look at the nozzle's influence on the simulation is important, as was found in the more global vantage point taken by Shur et al. [32,33]. An important item regarding modeling the nozzle, and implicit in the aforementioned studies, is the imposition of disturbances and the state of the boundary layer at the nozzle exit. SSS argue that the nozzle lip naturally provides a receptivity surface from which external disturbances, such as the upstream-traveling noise from the jet, scatter into vortical disturbances in the shear layer, promoting transition to turbulence some short distance downstream of the nozzle exit. However, in many of the experimental data (see Figs. 3b, 5b, and 7b), one observes that the axial root mean square fluctuations do not decay to zero as one approaches the nozzle exit, implying some fluctuation in the jet's mass flow rate. These effects have not been explicitly accounted for in the simulations and have not received much attention by experimenters. Their importance is not yet known. Thus, the issue is open whether including the nozzle without any additional disturbance introduction is sufficient, or if one needs to model the upstream flow unsteadiness also.

3) Closing the Ff-H and Kirchhoff surfaces: In discussions of both the Ffowcs Williams–Hawkings and Kirchhoff surface prediction methods for the far-field sound, it is apparent that the questions regarding their closure need to be answered. If the surfaces are left open, what are the quantitative errors? What are the errors associated with closing the surfaces in an ad hoc manner? Preferably, a consistent closing of the Ff-H surface needs to be addressed.

4) Comparisons between computation and experiment: One goal of this summary was to transparently present the computational data against corresponding experimental measurements. To accomplish this task it was necessary to use only a small subset of measurements, namely statistics of the centerline velocity and of the far-field sound. In attempting to uncover the trends, and their causes, additional information was needed. In many cases, more descriptive data, e.g., near-field turbulent spectra, were not available. As the simulations refine, more detailed reporting of the computational results, including spectra, cross-correlations, and so on will be necessary. Authors of both computational and experimental studies are encouraged to report as much detail as is feasible so that future comparisons can be more meaningfully made.

5) Increasing the bandwidth of the predictions: The limited bandwidth of the simulations is apparent. SSS noted that this limitation is very crucial when industrial use of LES for jet noise predictions is to be advocated, such as in evaluating chevron effectiveness. There are two main paths that have been discussed in the literature in this regard. The first involves development of a subgrid scale *noise* model which aims to estimate the missing noise from the unresolved scales using information from the resolved scales. This approach is under investigation by Bodony and Lele [100,101], and most recently by Bodony [102]. The second, and not necessarily orthogonal, path is to use thinner initial shear layers and provide more resolution in the near-nozzle region. The latter approach has a larger computational cost and it is not clear how much resolution one must provide to yield sufficiently high bandwidth predictions.

6) Low-speed heated jets: The current predictions of low-speed heated jets are seemingly very sensitive to the inflow conditions. Nor does there exist a suitable explanation for the cause. It is known that low-speed heated jets support a global, as opposed to convective, instability [103] and this may, if present in the simulations, adversely affect the predictions toward higher sound levels. Whether the simulations are exhibiting a global instability is not known.

VI. Conclusions

Based on the data presented herein, it is evident that the capability to accurately predict the near- and far-field properties of turbulent jets using large-eddy simulation has increased significantly. The numerical methods, and reasons for their use, are varied. The potential core length is not well predicted generally. When sufficiently thin initial shear layers ($\delta_\theta/D_j \sim 10^{-3}$) are used, the axial velocity mean and root mean square are within the experimental scatter to within an axial shift. In the acoustic far field, there is a ± 2 dB uncertainty in the LES predictions, predominantly due to associated uncertainties with the SGS model's influence, the method used to project the near-acoustic region outward, and the initial shear

layer thickness. At lower speeds, the predictive accuracy is not as good, especially when the jets are heated, with OASPL differences on the order of 5 dB. At higher speeds, the predictions are better (within 1 dB) for both heated and unheated jets.

There is no consensus regarding the subgrid model to use, if any is to be used at all, and what are the effects of the models. Arguments against using subgrid models are primarily motivated by reductions in computational cost, especially when upwinded schemes are used for dissipation of underresolved motions, but the case is also made regarding the influence of the SGS model on transition within the initial shear layers. This issue requires careful assessment because upwinded schemes can potentially dissipate intermediate scale fluctuations. It is vital that attention be paid to the dispersion and dissipation errors introduced by the numerical scheme, especially when considering the role of subgrid scale models. The far-field projection methods of Kirchhoff surfaces and Ffowcs Williams–Hawkings surfaces are commonly used, but how to close them properly remains unanswered.

Inflow conditions appear to be the dominant controlling factor in the predictive accuracy for the studies considered. For near-sonic and faster jets, inclusion of the nozzle geometry does not appear to yield more accurate predictions relative to a calculation with specified inlet conditions. At lower speeds, however, the explicit nozzle geometry has a beneficial effect. In the cases considered, the Reynolds number appeared as a parameter of secondary importance.

The future of jet noise predictions using LES appears to be secure, but the limited bandwidth of the predictions is of severe concern to its adoption for industrial use. It remains an open question how to increase the spectral bandwidth of the calculations while retaining reasonable computational cost. This problem is particularly important when the role of noise reduction concepts, such as chevrons, is to be investigated thoroughly.

Acknowledgments

Daniel J. Bodony gratefully acknowledges the Center for Turbulence Research, Stanford University, for support. Both authors sincerely thank C. Bailly and C. Bogey (École Centrale de Lyon), P. Spalart (The Boeing Company), M. Strelets (Federal Scientific Center, Applied Chemistry, St. Petersburg, Russia), N. Andersson (Volvo Aero Corporation), A. Lyrintzis (Purdue University), and P.-T. Lew (Purdue University) for the sharing of their data and for their contributions to this paper.

References

[1] Wang, M., Freund, J. B., and Lele, S. K., "Computational Prediction of Flow-Generated Sound," *Annual Review of Fluid Mechanics*, Vol. 38, 2006, pp. 483–512. doi:10.1146/annurev.fluid.38.050304.092036

[2] Lighthill, M. J., "On Sound Generated Aerodynamically 1: General Theory," *Proceedings of the Royal Society of London A*, Vol. 211, No. 1107, 1952, pp. 564–587. doi:10.1098/rspa.1952.0060

[3] Lighthill, M. J., "On Sound Generated Aerodynamically 2: Turbulence as a Source of Sound," *Proceedings of the Royal Society of London A*, Vol. 222, No. 1148, 1954, pp. 1–32. doi:10.1098/rspa.1954.0049

[4] Boersma, B. J., "Large Eddy Simulation of the Sound Field of a Round Turbulent Jet," *Theoretical and Computational Fluid Dynamics*, Vol. 19, No. 3, 2005, pp. 161–170. doi:10.1007/s00162-004-0107-7

[5] Kim, J., and Choi, H., "Effect of Initial Momentum Thickness on the Acoustic Source in an Incompressible Round Jet," *Presented at the 10th AIAA/CEAS Aeroacoustics Conference and Exhibit*, AIAA Paper 2004-2949, 2004.

[6] DeBonis, J. R., and Scott, J. N., "Large-Eddy Simulation of a Turbulent Compressible Round Jet," *AIAA Journal*, Vol. 40, No. 7, 2002, pp. 1346–1354.

[7] Loh, C. Y., and Hultgren, L. S., "Near-Field Noise Computation for a Supersonic Circular Jet," *Presented at the 11th AIAA/CEAS Aeroacoustics Conference*, AIAA Paper 2005-3042, 2005.

[8] Jansen, K., Maeder, T., and Reba, R., "Finite-Element Based Large-Eddy Simulation of the Near-Nozzle Region of a Compressible Round Jet," *Presented at the 8th AIAA/CEAS Aeroacoustics Conference*, AIAA Paper 2002-2358, 2002.

[9] Boersma, B. J., and Lele, S. K., "Large Eddy Simulation of a Mach 0.9 Turbulent Jet," *Presented at the 5th AIAA/CEAS Aeroacoustics Conference*, AIAA Paper 1999-1874, 1999.

[10] Constantinescu, G. S., and Lele, S. K., "Large Eddy Simulation of a Nearly Sonic Turbulent Jet and Its Radiated Noise," *Presented at the 39th Aerospace Sciences Meeting and Exhibit*, AIAA Paper 2001-0376, 2001.

[11] Tristanto, I. H., and Page, G. J., "Towards Hybrid Mesh Large Eddy Simulation for Jet Aeroacoustics," *Presented at the 10th AIAA/CEAS Aeroacoustics Conference*, AIAA Paper 2004-2933, 2004.

[12] Gröschel, E. R., Meike, M., and Schröder, W., "Noise Prediction for a Turbulent Jet Using an LES/CAA Method," *Presented at the 11th AIAA/CEAS Aeroacoustics Conference*, AIAA Paper 2005-3039, 2005.

[13] Gamet, L., and Estivalezes, J. L., "Application of Large-Eddy Simulations and Kirchhoff Method to Jet Noise Prediction," *AIAA Journal*, Vol. 36, No. 12, 1998, pp. 2170–2178.

[14] Bogey, C., Bailly, C., and Juvé, D., "Computation of the Sound Radiated by a 3-D Jet Using Large Eddy Simulation," *Presented at the 6th AIAA/CEAS Aeroacoustics Conference*, AIAA Paper 2000-2009, 2000.

[15] Freund, J. B., "Noise Sources in a Low-Reynolds-Number Turbulent Jet at Mach 0.9," *Journal of Fluid Mechanics*, Vol. 438, July 2001, pp. 277–305. doi:10.1017/S0022112001004414

[16] Stromberg, J. L., McLaughlin, D. K., and Troutt, T. R., "Flow Field and Acoustic Properties of a Mach Number 0.9 Jet at a Low Reynolds Number," *Journal of Sound and Vibration*, Vol. 72, No. 2, 1980, pp. 159–176. doi:10.1016/0022-460X(80)90650-1

[17] Bogey, C., Bailly, C., and Juvé, D., "Noise Investigation of a High Subsonic, Moderate Reynolds Number Jet Using a Compressible LES," *Theoretical and Computational Fluid Dynamics*, Vol. 16, No. 4, 2003, pp. 273–297. doi:10.1007/s00162-002-0079-4

[18] Zhao, W., Frankel, S. H., and Mongeau, L., "Large Eddy Simulations of Sound Radiation from Subsonic Turbulent Jets," *AIAA Journal*, Vol. 39, No. 8, 2001, pp. 1469–1477.

[19] Morris, P. J., Long, L. N., Scheidegger, T. E., and Boluriaan, S., "Simulations of Supersonic Jet Noise," *International Journal of Aeroacoustics*, Vol. 1, No. 1, 2002, pp. 17–41.

[20] Bodony, D. J., and Lele, S. K., "Large Eddy Simulation of Turbulent Jets and Progress Towards a Subgrid Scale Turbulence Model," *Proceedings of International Workshop on LES for Acoustics*, DLR Göttingen, Göttingen, Germany, 2002, pp. 1–12.

[21] Bogey, C., and Bailly, C., "LES of a High Reynolds, High Subsonic Jet: Effects of the Inflow Conditions on Flow and Noise," *Presented at the 9th AIAA/CEAS Aeroacoustics Conference and Exhibit*, AIAA Paper 2003-3170, 2003.

[22] Bogey, C., and Bailly, C., "Effects of Inflow Conditions and Forcing on Subsonic Jet Flows and Noise," *AIAA Journal*, Vol. 43, No. 5, 2005, pp. 1000–1007.

[23] Bogey, C., and Bailly, C., "LES of a High Reynolds, High Subsonic Jet: Effects of the Subgrid Modellings on Flow and Noise," *Presented at the 16th AIAA Computational Fluid Dynamics Conference*, AIAA Paper 2003-3557, 2003.

[24] Bogey, C., and Bailly, C., "Direct Computation of the Sound Radiated by a High-Reynolds Number, Subsonic Round Jet," *Presented at the CEAS Workshop From CFD to CAA*, Confederation of European Aerospace Societies Paper 2, 2002.

[25] Bogey, C., and Bailly, C., "Investigation of Subsonic Jet Noise Using LES: Mach and Reynolds Number Effects," *Presented at the 10th AIAA/CEAS Aeroacoustics Conference*, AIAA Paper 2004-3023, 2004.

[26] Andersson, N., Eriksson, L.-E., and Davidson, L., "Large-Eddy Simulation of a Mach 0.75 Jet," *Presented at the 9th AIAA/CEAS Aeroacoustics Conference and Exhibit*, AIAA Paper 2003-3312, 2003.

[27] Andersson, N., Eriksson, L.-E., and Davidson, L., "Investigation of an Isothermal Mach 0.75 Jet and Its Radiated Sound Using Large-Eddy Simulation and Kirchhoff Surface Integration," *International Journal of Heat and Fluid Flow*, Vol. 26, No. 3, 2005, pp. 393–410. doi:10.1016/j.ijheatfluidflow.2004.09.004

[28] Andersson, N., Eriksson, L.-E., and Davidson, L., "A Study of Mach 0.75 Jets and Their Radiated Sound Using Large-Eddy Simulation," *Presented at the 10th AIAA/CEAS Aeroacoustics Conference and Exhibit*, AIAA Paper 2004-3024, 2004.

[29] Andersson, N., Eriksson, L.-E., and Davidson, L., "Large-Eddy Simulation of Subsonic Turbulent Jets and Their Radiated Sound," *AIAA Journal*, Vol. 43, No. 9, 2005, pp. 1899–1912.
[30] Andersson, N., Eriksson, L.-E., and Davidson, L., "Effects of Inflow Conditions and Subgrid Model on LES for Turbulent Jets," *Presented at the 11th AIAA/CEAS Aeroacoustics Conference and Exhibit*, AIAA Paper 2005-2925, 2005.
[31] Shur, M., Spalart, P. R., and Strelets, M. K., "Noise Prediction for Increasingly Complex Jets," *Presented at the Computational Aeroacoustics: From Acoustic Sources Modeling to Far-Field Radiated Noise Prediction Colloquium EUROMECH 449*, European Mechanics Society, 2003.
[32] Shur, M., Spalart, P. R., and Strelets, M. K., "Noise Prediction for Increasingly Complex Jets, Part 1: Methods and Tests," *International Journal of Aeroacoustics*, Vol. 4, Nos. 3–4, 2005, pp. 213–246. doi:10.1260/1475472054771376
[33] Shur, M., Spalart, P. R., and Strelets, M. K., "Noise Prediction for Increasingly Complex Jets, Part 2: Applications," *International Journal of Aeroacoustics*, Vol. 4, Nos. 3–4, 2005, pp. 247–266. doi:10.1260/1475472054771385
[34] Bodony, D. J., and Lele, S. K., "Jet Noise Prediction of Cold and Hot Subsonic Jets Using Large-Eddy Simulation," *Presented at the 10th AIAA/CEAS Aeroacoustics Conference*, AIAA Paper 2004-3022, 2004.
[35] Bodony, D. J. and Lele, S. K., "On Using Large-Eddy Simulation for the Prediction of Noise from Cold and Heated Turbulent Jets," *Physics of Fluids*, Vol. 17, No. 085103, 2005, pp. 1–20.
[36] Uzun, A., Blaisdell, G. A., and Lyrintzis, A. S., "3-D Large Eddy Simulation for Jet Aeroacoustics," *Presented at the 9th AIAA/CEAS Aeroacoustics Conference*, AIAA Paper 2003-3322, 2003.
[37] Uzun, A., Lyrintzis, A. S., and Blaisdell, G. A., "Coupling of Integral Acoustics Methods with LES for Jet Noise Prediction," *Presented at the 42nd AIAA Aerospace Sciences Meeting and Exhibit*, AIAA Paper 2004-0517, 2004.
[38] Uzun, A., Blaisdell, G. A., and Lyrintzis, A. S., "Application of Compact Schemes to Large Eddy Simulations of Turbulent Jets," *Journal of Scientific Computing*, Vol. 21, No. 3, 2004, pp. 283–319. doi:10.1007/s10915-004-1319-0
[39] Uzun, A., Lyrintzis, A. S., and Blaisdell, G. A., "Coupling of Integral Acoustics Methods with LES for Jet Noise Prediction," *International Journal of Aeroacoustics*, Vol. 3, No. 4, 2004, pp. 297–346. doi:10.1260/1475472043499290
[40] Lew, P., Uzun, A., Blaisdell, G. A., and Lyrintzis, A. S., "Effects of Inflow Forcing on Jet Noise Using Large Eddy Simulation," *Presented at the 42nd AIAA Aerospace Sciences Meeting and Exhibit*, AIAA Paper 2004-0516, 2005.
[41] Lew, P., Blaisdell, G. A., and Lyrintzis, A. S., "Recent Progress of Hot Jet Aeroacoustics Using 3-D Large-Eddy Simulation," *Presented at the 11th AIAA/CEAS Aeroacoustics Conference*, AIAA Paper 2005-3084, 2005.
[42] Wu, X., Tristanto, I. H., Page, G. J., and McGuirk, J. J., "Influence of Nozzle Modelling in LES of Turbulent Free Jets," *Presented at the 11th AIAA/CEAS Aeroacoustics Conference*, AIAA Paper 2005-2883, 2005.
[43] Shur, M. L., Spalart, P. R., Strelets, M. K., and Garbaruk, A. V., "Further Steps in LES-Based Noise Prediction for Complex Jets," *Presented at the 44th AIAA Aerospace Sciences Meeting and Exhibit*, AIAA Paper 2006-0485, 2006.
[44] Colonius, T., and Lele, S. K., "Computational Aeroacoustics: Progress on Nonlinear Problems of Sound Generation," *Progress in Aerospace Sciences*, Vol. 40, No. 6, 2004, pp. 345–416. doi:10.1016/j.paerosci.2004.09.001
[45] Lele, S. K., "Compact Finite Difference Schemes with Spectral-Like Resolution," *Journal of Computational Physics*, Vol. 103, No. 1, 1992, pp. 16–42. doi:10.1016/0021-9991(92)90324-R
[46] Lui, C., and Lele, S. K., "Direct Numerical Simulation of Spatially Developing, Compressible, Turbulent Mixing Layers," *Presented at the 39th AIAA Aerospace Sciences Meeting and Exhibit*, AIAA Paper 2001-0291, 2001.
[47] Tam, C. K. W. and Webb, J. C., "Dispersion-Relation-Preserving Finite Difference Schemes for Computational Acoustics," *Journal of Computational Physics*, Vol. 107, No. 2, 1993, pp. 262–281. doi:10.1006/jcph.1993.1142
[48] Bogey, C., and Bailly, C., "A Family of Low Dispersive and Low Dissipative Explicit Schemes for Flow and Noise Computations," *Journal of Computational Physics*, Vol. 194, No. 1, 2004, pp. 194–214. doi:10.1016/j.jcp.2003.09.003
[49] Roe, P. L., "Approximate Rieman Solvers, Parameter Vectors, and Difference Schemes," *Journal of Computational Physics*, Vol. 43, No. 2, 1981, pp. 357–378. doi:10.1016/0021-9991(81)90128-5
[50] Hirsch, C., *Numerical Computation of Internal and External Flows*, Vol. 2, Wiley, New York, 1990.
[51] Hu, F. Q., Hussaini, M. Y., and Manthey, J. L., "Low-Dissipation and Low-Dispersion Runge-Kutta Schemes for Computational Acoustics," *Journal of Computational Physics*, Vol. 124, No. 1, 1996, pp. 177–191. doi:10.1006/jcph.1996.0052
[52] Meneveau, C., and Katz, J., "Scale-Invariance and Turbulence Models for Large-Eddy Simulation," *Annual Review of Fluid Mechanics*, Vol. 32, 2000, pp. 1–32. doi:10.1146/annurev.fluid.32.1.1
[53] Smagorinsky, J., "General Circulation Experiments with the Primitive Equations, 1: The Basic Experiment," *Monthly Weather Review*, Vol. 91, No. 3, 1963, pp. 99–164. doi:10.1175/1520-0493(1963)091<0099:GCEWTP>2.3.CO;2
[54] Erlebacher, G., Hussaini, M., Speziale, C., and Zang, T., "Toward the Large-Eddy Simulation of Compressible Turbulent Flows," *Journal of Fluid Mechanics*, Vol. 238, May 1992, pp. 155–185. doi:10.1017/S0022112092001678
[55] Germano, M., Piomelli, U., Moin, P., and Cabot, W. H., "A Dynamic Subgrid-Scale Eddy Viscosity Model," *Physics of Fluids A*, Vol. 3, No. 7, 1991, pp. 1760–1765. doi:10.1063/1.857955
[56] Moin, P., Squires, K., Cabot, W., and Lee, S., "A Dynamic Subgrid-Scale Model for Compressible Turbulence and Scalar Transport," *Physics of Fluids A*, Vol. 3, No. 11, 1991, pp. 2746–2757. doi:10.1063/1.858164
[57] Salvetti, M., and Banerjee, S., "A Priori Tests of a New Dynamic Subgrid-Scale Model for Finite Difference Large-Eddy Simulation," *Physics of Fluids*, Vol. 7, No. 11, 1995, pp. 2831–2847. doi:10.1063/1.868779
[58] Visbal, M. R., and Gaitonde, D. V., "On the Use of Higher-Order Finite-Difference Schemes on Curvilinear and Deforming Meshes," *Journal of Computational Physics*, Vol. 181, No. 1, 2002, pp. 155–185. doi:10.1006/jcph.2002.7117
[59] Fureby, C., and Grinstein, F. F., "Monotonically Integrated Large Eddy Simulation of Free Shear Flows," *AIAA Journal*, Vol. 37, No. 5, 1999, pp. 544–556.
[60] Colonius, T., "Modeling Artificial Boundary Conditions for Compressible Flow," *Annual Review of Fluid Mechanics*, Vol. 36, 2004, pp. 315–345. doi:10.1146/annurev.fluid.36.050802.121930
[61] Tam, C. K. W., and Dong, Z., "Radiation and Outflow Boundary Conditions for Direct Computation of Acoustic and Flow Disturbances in a Nonuniform Mean Flow," *Journal of Computational Acoustics*, Vol. 4, No. 2, 1996, pp. 175–201. doi:10.1142/S0218396X96000040
[62] Bogey, C., and Bailly, C., "Three-Dimensional Non-Reflective Boundary Conditions for Acoustic Simulations: Far Field Formulation and Validation Test Cases," *Acta Acoustica*, Vol. 88, No. 4, 2002, pp. 463–471.
[63] Poinsot, T. J., and Lele, S. K., "Boundary Conditions for Direct Simulations of Compressible Viscous Flows," *Journal of Computational Physics*, Vol. 101, No. 1, 1992, pp. 104–129. doi:10.1016/0021-9991(92)90046-2
[64] Bodony, D. J., "Analysis of Sponge Zones for Computational Fluid Mechanics," *Journal of Computational Physics*, Vol. 212, No. 2, 2006, pp. 681–702. doi:10.1016/j.jcp.2005.07.014
[65] Babu, P. C., and Mahesh, K., "Upstream Entrainment in Numerical Simulations of Spatially Evolving Round Jets," *Physics of Fluids*, Vol. 16, No. 10, 2004, pp. 3699–3705. doi:10.1063/1.1780548
[66] Huerre, P., and Monkewitz, P. A., "Absolute and Convective Instabilities in Free Shear Layers," *Journal of Fluid Mechanics*, Vol. 159, Oct. 1985, pp. 151–168. doi:10.1017/S0022112085003147
[67] Lesshafft, L., Huerre, P., Sagaut, P., and Terracol, M., "Nonlinear Global Modes in Hot Jets," *Journal of Fluid Mechanics*, Vol. 554, May 2006, pp. 393–409. doi:10.1017/S0022112006008974
[68] Bodony, D. J., and Lele, S. K., "Applications and Results for Large-Eddy Simulations for Acoustics: Far-field Jet Acoustics," *LES for Acoustics*, edited by C. Wagner, T. Hüttl, and P. Sagaut, Cambridge Univ. Press, Cambridge, England, U.K., 2005, pp. 289–310.

[69] Tam, C. K. W., "Supersonic Jet Noise," *Annual Review of Fluid Mechanics*, Vol. 27, 1995, pp. 17–43. doi:10.1146/annurev.fl.27.010195.000313
[70] Soh, W. Y., "Unsteady Jet Flow Computation Towards Noise Prediction," *Presented at the 32nd AIAA Aerospace Sciences Meeting and Exhibit*, AIAA Paper 94-0138, 1994.
[71] Lyrintzis, A. S., and Mankbadi, R. R., "On the Prediction of the Far-Field Jet Noise Using Kirchhoff's Formulation," *Presented at the 33rd AIAA Aerospace Sciences Meeting and Exhibit*, AIAA Paper 95-0508, 1995.
[72] Viswanathan, K., "Analysis of the Two Similarity Components of Turbulent Mixing Noise," *AIAA Journal*, Vol. 40, No. 9, 2002, pp. 1735–1744.
[73] Pilon, A. R., and Lyrintzis, A. S., "Integral Methods for Computational Aeroacoustics," AIAA Paper 1997-0020, 1997.
[74] Pilon, A. R., and Lyrintzis, A. S., "Development of an Improved Kirchhoff Method for Jet Aeroacoustics," *AIAA Journal*, Vol. 36, No. 5, 1998, pp. 783–790.
[75] Freund, J. B., Lele, S. K., and Moin, P., "Calculation of the Radiated Sound Field Using an Open Kirchhoff Surface," *AIAA Journal*, Vol. 34, No. 5, 1996, pp. 909–916.
[76] Evans, L. C., *Partial Differential Equations*, American Mathematical Society, Providence, RI, 1998.
[77] Brentner, K. S., and Farassat, F., "An Analytical Comparison of the Acoustic Analogy and Kirchhoff Formulation for Moving Surfaces," *AIAA Journal*, Vol. 36, No. 8, 1998, pp. 1379–1386.
[78] Ffowcs Williams, J. E., and Hawkings, D. L., "Sound Generation by Turbulence and Surfaces in Arbitrary Motion," *Proceedings of the Royal Society of London A*, Vol. 264, No. 1151, 1969, pp. 321–342. doi:10.1098/rsta.1969.0031
[79] Crighton, D. G., Dowling, A. P., Ffowcs Williams, J. E., Heckl, M., and Leppington, F. G., *Modern Methods in Analytical Acoustics*, Springer–Verlag, New York, 1996.
[80] Wang, M., Lele, S. K., and Moin, P., "Computation of Quadrupole Noise Using Acoustic Analogy," *AIAA Journal*, Vol. 34, No. 11, 1996, pp. 2247–2254.
[81] Tanna, H. K., "An Experimental Study of Jet Noise Part 1: Turbulent Mixing Noise," *Journal of Sound and Vibration*, Vol. 50, No. 3, 1977, pp. 405–428. doi:10.1016/0022-460X(77)90493-X
[82] Crighton, D. G., "Acoustics as a Branch of Fluid Mechanics," *Journal of Fluid Mechanics*, Vol. 106, May 1981, pp. 261–298. doi:10.1017/S0022112081001602
[83] Viswanathan, K., "Aeroacoustics of Hot Jets," *Journal of Fluid Mechanics*, Vol. 516, Oct. 2004, pp. 39–82. doi:10.1017/S0022112004000151
[84] Lau, J. C., "Effects of Exit Mach Number and Temperature on Mean-Flow and Turbulence Characteristics in Round Jets," *Journal of Fluid Mechanics*, Vol. 105, April 1981, pp. 193–218. doi:10.1017/S0022112081003170
[85] Bridges, J., and Wernet, M. P., "Measurements of the Aeroacoustic Sound Source in Hot Jets," *Presented at the 9th AIAA/CEAS Aeroacoustics Conference and Exhibit*, AIAA Paper 2003-3130, 2003.
[86] Ahuja, K. K., Lepicovsky, J., Tam, C. K. W., Morris, P. J., and Burrin, R. H., "Tone-Excited Jet: Theory and Experiments," NASA TR NASA CR-3538, Nov. 1982.
[87] Lau, J. C., Morris, P. J., and Fisher, M. J., "Measurements in Subsonic and Supersonic Free Jets Using a Laser Velocimeter," *Journal of Fluid Mechanics*, Vol. 93, No. 1, 1979, pp. 1–27. doi:10.1017/S0022112079001750
[88] Ahuja, K. K., "Correlation and Prediction of Jet Noise," *Journal of Sound and Vibration*, Vol. 29, No. 2, 1973, pp. 155–168. doi:10.1016/S0022-460X(73)80132-4
[89] Tam, C. K. W., "Jet Noise: Since 1952," *Theoretical and Computational Fluid Dynamics*, Vol. 10, Nos. 1–4, 1998, pp. 393–405. doi:10.1007/s001620050072
[90] Viswanathan, K., and Clark, L. T., "Effect of Nozzle Internal Contour on Jet Aeroacoustics," *International Journal of Aeroacoustics*, Vol. 3, No. 2, 2004, pp. 103–135. doi:10.1260/1475472041494819
[91] Crow, S. C., and Champagne, F. H., "Orderly Structure in Jet Turbulence," *Journal of Fluid Mechanics*, Vol. 48, Aug. 1971, pp. 547–591. doi:10.1017/S0022112071001745
[92] Bodony, D. J., "Aeroacoustics of Turbulent Free Shear Flows," Ph.D. Thesis, Stanford Univ., Stanford, CA, Dec. 2004.
[93] Michalke, A., "Survey on Jet Instability Theory," *Progress in Aerospace Sciences*, Vol. 21, 1984, pp. 159–199. doi:10.1016/0376-0421(84)90005-8
[94] Bogey, C., and Bailly, C., "Decrease of the Effective Reynolds Number with Eddy-Viscosity Subgrid Modeling," *AIAA Journal*, Vol. 43, No. 2, 2005, pp. 437–439.
[95] Uzun, A., Blaisdell, G. A., and Lyrintzis, A. S., "Sensitivity to the Smagorinsky Constant in Turbulent Jet Simulations," *AIAA Journal*, Vol. 41, No. 10, 2003, pp. 2077–2079.
[96] Uzun, A., Blaisdell, G. A., and Lyrintzis, A. S., "Impact of Subgrid-Scale Models on Jet Turbulence and Noise," *AIAA Journal*, Vol. 44, No. 6, 2006, pp. 1365–1368.
[97] Bogey, C., and Bailly, C., "Large Eddy Simulations of Transitional Round Jets: Influence of the Reynolds Number on Flow Development and Energy Dissipation," *Physics of Fluids*, Vol. 18, No. 065101, 2006, pp. 1–14.
[98] Uzun, A., and Hussaini, M. Y., "High Frequency Noise Generation in the Near-Nozzle Region of a Jet," *Presented at the 12th AIAA/CEAS Aeroacoustics Conference*, AIAA Paper 2006-2499, 2006.
[99] Barré, S., Bogey, C., and Bailly, C., "Computation of the Noise Radiated by Jets with Laminar/Turbulent Nozzle-Exit Conditions," *Presented at the 12th AIAA/CEAS Aeroacoustics Conference*, AIAA Paper 2006-2443, 2006.
[100] Bodony, D. J., and Lele, S. K., "Spatial Scale Decomposition of Shear Layer Turbulence and the Sound Sources Associated with the Missing Scales in a Large-Eddy Simulation," *Presented at the 8th AIAA/CEAS Aeroacoustics Conference*, AIAA Paper 2002-2454, 2002.
[101] Bodony, D. J., and Lele, S. K., "A Stochastic Subgrid Scale Noise Model for Noise Predictions of Subsonic Jets," *Presented at the 9th AIAA/CEAS Aeroacoustics Conference*, AIAA Paper 2003-3252, 2003.
[102] Bodony, D. J., "Developing a Subgrid Scale Noise Model for Use with Large-Eddy Simulation," *Annual Research Briefs*, Center for Turbulence Research, Stanford, CA, 2005.
[103] Monkewitz, P. A., Bechert, D. W., Barsikow, B., and Lehmann, B., "Self-Excited Oscillations and Mixing in a Heated Round Jet," *Journal of Fluid Mechanics*, Vol. 213, April 1990, pp. 611–639. doi:10.1017/S0022112090002476
[104] Arakeri, V. H., Krothapalli, A., Siddavaram, V., Alkislar, M., and Lourenco, L., "On the Use of Microjets to Suppress Turbulence in a Mach 0.9 Axisymmetric Jet," *Journal of Fluid Mechanics*, Vol. 490, Sept. 2003, pp. 75–98. doi:10.1017/S0022112003005202

C. Bailly
Associate Editor